Predictive Risk Analysis for Leakage Accidents with Dynamic Behaviour

Xiangyu Kong [a, b], Ruishu Huang [c], He Li [b, d], Jichuan Kang [e, *], Yan Dong [a, e], C. Guedes Soares [b], Jin Wang [d]

[a] *Yantai Research Institute of Harbin Engineering University, Harbin Engineering University, Yantai, China*

[b] *Centre for Marine Technology and Ocean Engineering (CENTEC), Instituto Superior Técnico, Universidade de Lisboa, Lisbon, Portugal.*

[c] *College of Letters & Science, University of Wisconsin-Madison, Madison, United States*

[d] *School of Engineering, Liverpool John Moores University, Liverpool, 3 Byrom Street, L3 3AF, UK*

[e] *College of Shipbuilding Engineering, Harbin Engineering University, Harbin, China*

Abstract: A predictive risk analysis approach is proposed for modelling leakage accidents with dynamic behaviour based on time-series simulations in order to enhance data foundation of risk analysis tasks. Critical failure items are first identified by the Failure Model and Effects Analysis model and the occurrence probabilities of which are subsequently computed by the Bayesian and Event Tree Analysis methods. The dynamic behaviour of the accidents is simulated to reveal their time-series failure consequences. With the probabilities and consequences obtained, a predictive risk analysis approach is established as a basis to calculate the risk index of accidents with the consideration of dynamic behaviours. The applicability and superior performance of the proposed approach are illustrated by a leakage risk analysis of offshore hydrogen storage systems. Overall, the proposed approach extends the existing inductive risk analysis concepts to predictive patterns and contributes to leakage accidents analysis and prevention with the situation of data and knowledge scarcities.

Keywords: Offshore hydrogen storage system; Failure mode and effect analysis; Bayesian theory; Long short-term memory; Dynamic failure behaviour

* Corresponding author: kangjichuan@hrbeu.edu.cn (Jichuan Kang)

1. Introduction

Hydrogen generation by offshore wind is a promising solution for variable energy storage, which allows offshore wind farms to expand into deeper and further waters [1]. This new concept can partly substitute long cables connecting far offshore wind farms and the grid onshore but will bring additional risks in terms of hydrogen safety [2]. For instance, leakage accidents (e.g., hydrogen leakage) pose significant threats due to their physical properties such as the flammability of hydrogen [3]. These leakage accidents present dynamic adverse effects across spatial and temporal scales, with extended hazardous consequences and variable occurrence probabilities [4]. To this end, one of the keys for the development and deployment of hydrogen generation by offshore wind is to overcome safety issues through avoiding leakage accidents [5].

Leakage risk analysis includes probability analysis and consequence assessment [6]. Qualitative, quantitative, and semi-quantitative risk analysis concepts are based on existing human experiences, mathematical models, simulation tools, and statistical analyses [7]. These strategies quantify the uncertainty and impact of accidents, allowing decision-makers to prioritize and control risk factors before their occurrence [8]. Probability analysis quantifies the likelihood of risk factors according to objective or subjective data as a basis to identify hazards and prioritize the associated potential risks [9]. Two solutions have been applied to approximate the likelihood of leakage risk factors: inductive approaches and leak-size-based modelling methods [10].

Inductive approaches access probabilities of risk factors using Fault Tree Analysis (FTA), statistical methods such as Bayesian theory, intelligent methods, etc. For instance, Casamirra et al. [11] applied the FTA approach to update the leakage probability of storage tanks based on failure data from similar products. Although FTA is widely used to identify system weak links from a probability perspective, its accuracy is constrained by static system assumptions. Feng et al. [12] developed a vibration-based digital twin method for risk factors monitoring and prediction. It offers a practical framework for applying digital twin technology in real-world industrial prognostics and risk control. Wei et al. [13] proposed a global adaptive modal-data interaction prognostic framework for system risk analysis and prediction, which provide the sector with a superior model for operational risk prognosis. Durga et al.

[14] developed a dynamic FTA that models failure dynamics and simultaneously solves large-scale modelling problems. Subsequently, Bayesian Networks (BNs) are introduced to represent dependent failures in complex systems by identifying and modelling correlations among root causes. For instance, Meng et al. [15] proposed a physics-informed data-driven BN for accident risk analysis that captures correlated failures from data and model perspectives. Additionally, Event Tree Analysis (ETA) [16], statistical model [17], and Bayesian model [18] have been developed to acquire occurrence probabilities of leakage risk factors as well. It is worth noting that the estimation of leakage probability relies on sufficient data which will turn out to be disabled in the case of insufficient data situations (a common situation in real engineering cases).

On the other hand, leak-size-based methods provide an alternative to estimate leakage probabilities under data scarcity and limited subjective experience. For instance, Spouge [19] developed a leak size-based model to form standardized leakage probabilities for offshore devices. The results revealed that incorporating leak size factors can improve the accuracy of leakage probability estimation. LaChance et al. [20] proposed a Bayesian model to predict the leakage probability, in which the leakage probability is modelled as a function of leak sizes. Zhang et al. [21] developed an inspection policy optimisation method, which can effectively reduce decision-related risks by accounting for uncertainties in both system state and inspection decision-making. Zheng et al. [22] combined a time-varying discrete dynamic BN with a tailored Hungarian algorithm, which significantly improves the credibility of risk assessment of complex systems. The proposed approach enables accurate reliability estimation and provides deeper insights into the optimal allocation of support among components. Bi et al. [23] proposed an innovative inverse neural-network-based stochastic model calibration framework that converts high-dimensional sequential responses into RGB image representations, offering a new paradigm for real-time calibration of complex engineering systems. Ji et al. [24] proposed a leakage localisation model for subsea pipelines, which significantly improve leakage localisation accuracy by 15.65%. Hecht et al. [25] applied the Bayesian model to estimate the leakage probability of gas bunkering systems, which required complex modelling procedures and vast computations. The mentioned issues are then partially addressed by the Hierarchical Bayesian Model (HBM).

It is pointed out that the core for risk analysis of leakage, applies to both inductive approaches and leak-size-based methods, is the consequence analysis, which mainly focuses on evaluating the potential impacts of accidents on safety, environmental, and economic losses by single-model-based approaches and integrated-model-based methodologies [26-28]. Specifically, (i) Single-model-based methods apply a single approach, such as an empirical and a simulation model, to assess the consequences of leakage [29,30]. Empirical models such as Gaussian model, SLAB model, and Ermak model are typical tools for consequence analysis, which are advantageous but unable to process complex or dynamic failures. Alternatively, Computational Fluid Dynamics (CFD) such as PHAST, FLUENT, and FLACS have been developed for the consequence analysis but the analytical accuracy of the these methods is limited; (ii) Integrated-model-based methodologies incorporate several methods to get free from the limitations of a single model. For example: FLACS incorporates Latin Hypercube Sampling (LHS) and Monte Carlo method improves coverage [31]; Empirical functions are incorporated to improve the accuracy of the simulation results [32]; Surrogate models are able to reduce computation time spent in solving the complex mathematical models. To be specific, Ning et al. [33] combined convolutional neural networks and spectrum enhancement to predict gas pipeline leakage positions to improve the accuracy and efficiency of leakage detection. Kopbayev et al. [34] combined the CFD and a Long Short-Term Memory (LSTM) model to perform leakage diagnosis, releasing the dependence of risk diagnosis on sensor data. In addition, Zhang et al. [35] developed a reliable wave-basin experimental system to obtain time-series data of complex offshore systems under representative conditions for risk analysis. Similar artificial intelligence-based and simulation-based methods leakage risk analysis methods can be seen in [36] and [37].

The above-mentioned post-event analysis approaches are, however, particularly suitable for risk analysis with sufficient historical data [38], which fail to reflect current and future risks. It is critical to note that the time-series nature of leakage-related hazards (e.g., offshore hydrogen leaks) renders the risk factors dynamic. Given this, the prediction of time-series leakage consequence becomes necessary for a better understanding towards accident escalation and mitigation, providing forward-looking insights into the development of leakage risk as well as prevention actions. Moreover, the availability of time-series accident data poses a challenging, as direct observation of risk progression

are typically unavailable prior to accident occurrence. Data limitation further restricts the applicability of existing data-driven post-event methods and calls for predictive frameworks to reveal the dynamic behaviour of leakage accidents.

To this end, this paper proposes a predictive risk analysis approach for accidents with dynamic behaviour with the assistance of time-series simulations, aiming to provide predictive risk analysis to better support the accident analysis, prediction, and prevention. Overall, the proposed method includes critical risk item identification, accident probability computation, and simulation-based predictive risk analysis. The main contributions of this paper are listed below:

- To propose a predictive risk analysis approach to assess the time-series and evolutionary risks of accidents with dynamic behaviour, supporting the proactive prevention and forward-looking risk management.
- To propose a failure probability updating model to reveal failure features of dynamic accidents.
- To propose a Deep Neural Network (DNN) and LSTM combined model to predict the potential dynamic behaviour (time-series consequence) of leakage consequence before accidents occurrence.

The remainder of this paper is organized as follows. Section 2 introduces the proposed predictive risk analysis methodology. Section 3 provides the results and discussion of the case study of an offshore hydrogen storage system. Section 4 gives conclusions.

2. Methodology

The purpose of this study is to predict the dynamic behaviour of hydrogen leakage accidents, defined as the spatiotemporal evolution of hydrogen leakage concentration, with the DNN model capturing spatial evolution and LSTM model capturing temporal evolution. The proposed predictive risk analysis framework, taking the leakage risk analysis of an offshore hydrogen storage system as an example, consists of four modules. The framework is shown in Figure 1, where (i) the proactive Failure Mode and Effect Analysis (FMEA) model determines the critical items; (ii) the information-driven HBM updates leakage probabilities; (iii) the consequence predictive model predicts time-series leakage

consequences and (iv) the time-series risk analysis defines hazard zones. It is specifically described as follows:

Step #1: Decompose the system into components and identify critical components through FMEA, as described in Section 2.1.

Step #2: Acquire the leakage probability of critical components from the targeted offshore hydrogen storage system (if data is available) or from similar systems (if data is insufficient). Define a group of credible leakage scenarios based on the LHS technique.

Step #3: Update the leakage probability of critical components using the leakage probability collected in Step 2 and prior information based on BHM, as described in Section 2.2.

Step #4: Estimate the probability of fire and explosion accidents using the ETA, as described in Section 2.2.

Step #5: Simulate leakage accidents and collect hydrogen leakage concentrations, as described in Section 2.3.

Step #6: Simulate the consequences of accidents (e.g. fires and explosions) using the data from Step #5. Collect data on heat radiation and overpressure.

Step #7: Develop and train a DNN model using training data collected from Step #2 and Step #5, to predict critical leakage positions, as described in Section 2.3.

Step #8: Develop and train a LSTM model using time-series data of leakage concentrations at the critical leakage positions, to predict time-series leakage concentration, as described in Section 2.3.

Step #9: Assess time-series leakage risk based on updated leakage probabilities and predicted time-series leakage concentrations, as described in Section 2.4.

Step #10: Assess the risks of fires and explosions by combining the calculated occurrence probabilities with the simulated consequences, as described in Section 2.4.

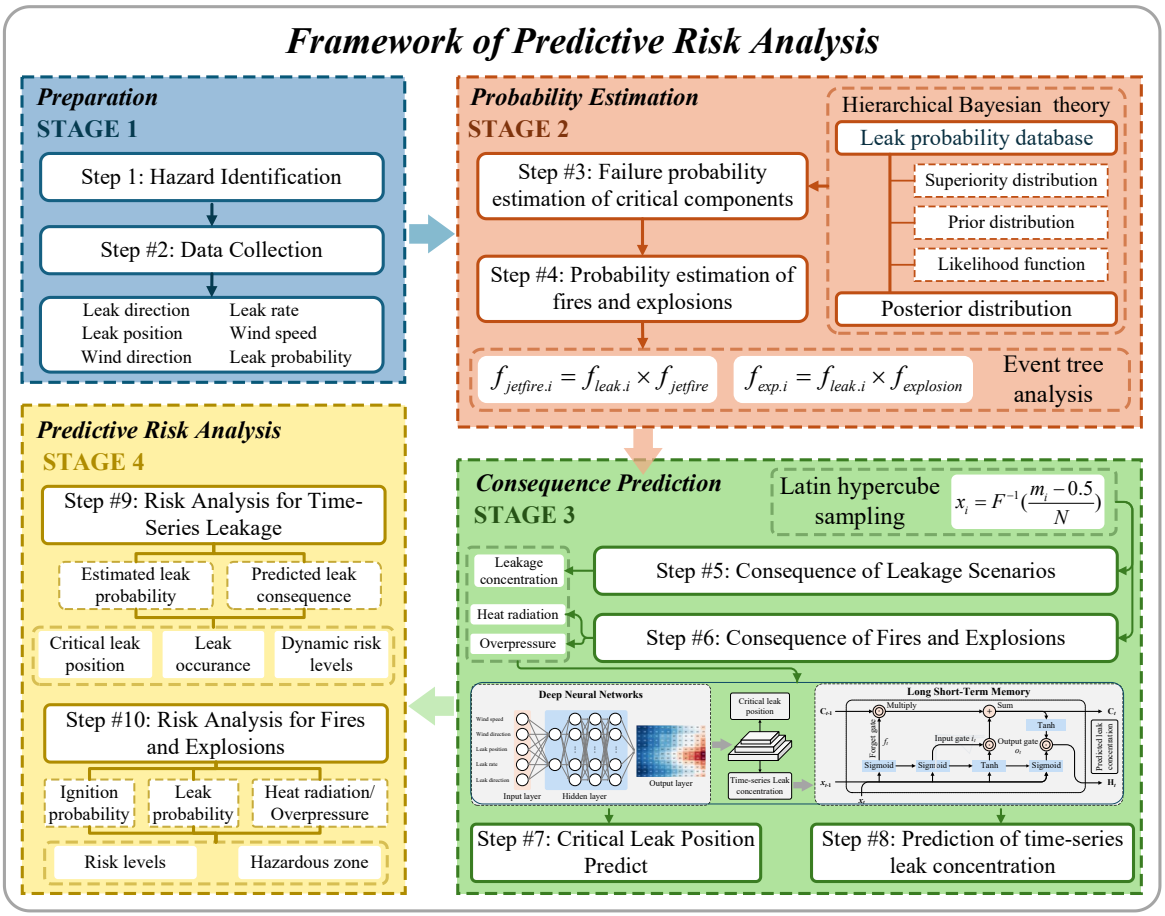

Figure 1. The proposed predictive risk analysis framework.

2.1. Critical component identification

Several methods are available for the identification of critical components and for the characterization of leakage hazards. The FMEA method is applied to analyse potential failure items (e.g., failure modes, failure causes, and components) in this paper. FMEA is an important method for hazard identification and prevention of complex systems. Recent decades have seen extensive developments and applications of FMEA in hazard identification of complex systems. FMEA relies on an exhaustive review of items within each layer and maps connections between items in various layers according to their affiliations [39]. With vertical extension across layers (e.g., from the system level to root causes) and horizontal expansion within each layer through an exhaustive review of items, a systematic decomposition and a comprehensive knowledge graph of systems can be formulated to understand the system's configuration and behaviour in terms of failures, improvements, quality control, and other dimensions [40].

Numerically, FMEA assigns an index to each item such as the Risk Priority Number (RPN) to reflect the relative importance of items in each layer. With the indices of items computed, items are ranked in descending order based on their criticality, and the top-ranked items are further analysed and controlled [41]. Specifically, FMEA determines critical system items through quantitative combinations of Severity (S), Occurrence (O), and Detection (D) [42]:

$$RPN = Severity \times Occurrence \times Detection \tag{1}$$

where *Severity* represents the impacts of an item on the system; *Occurrence* is the likelihood of an item to happen; *Detection* reflects the difficulty of detecting the item in advance. The use of subjective evidence reduces the requirements for objective failure data and makes FMEA user-friendly. To this end, the FMEA structure is applied as the foundation of failure analysis models developed in this study.

2.2. Probability estimation

The leakage probability of critical components is updated by HBM, and the probabilities of fire and explosion are computed using ETA. First, HBM is used to integrate prior information and available data for updating beliefs about estimated parameters HBM consists of the hyperprior distribution, prior distribution ($p(\alpha)$), likelihood function ($p(x|\alpha)$), and posterior distribution ($p(\alpha|x)$), as shown in Figure 2. Available data are used to establish the likelihood function, which is informed by hyperprior and prior distributions. Suitable statistical models (e.g., Uniform and Normal distributions) are applied to establish hyperprior and prior distributions. The hyperprior distribution provides adaptive adjustments and optimisation of priors. Accordingly, the posterior distributions of estimated parameters can be calculated as [19]:

$$p(\alpha|x) = \frac{p(x|\alpha)\,p(\alpha)}{p(x)} = \frac{p(x|\alpha)\,p(\alpha)}{\int p(x|\alpha)p(\alpha)\,d\alpha} \tag{2}$$

where α denotes the estimated parameters; x denotes the observed data; $p(x)$ denotes a normalisation function ensuring that the parameter estimates are bounded between zero and one.

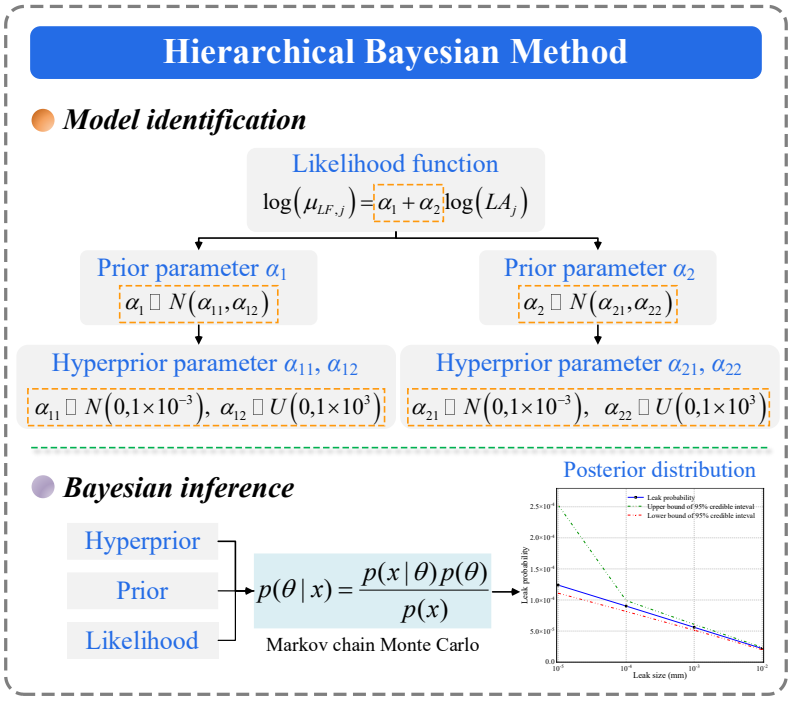

Figure 2. The framework of the hierarchical Bayesian model.

Secondly, ETA is used to estimate the occurrence probabilities of fire and explosion accidents based on the ignition timing. According to [43], immediate ignition of released flammable gas leads to jet fires, whose probability is expressed as [19]:

$$f^i_{\text{jetfire}} = f^i_{\text{leak}} \times f_{\text{jetfire}} \tag{3}$$

Delayed ignition allows the released flammable gas to disperse and form a combustible cloud, which triggers an explosion upon subsequent ignition. The probability of an explosion is calculated as [19]:

$$f^i_{\text{explosion}} = f^i_{\text{leak}} \times f_{\text{explosion}} \tag{4}$$

where f_{jetfire}, $f_{\text{explosion}}$, and f^i_{leak} denote the occurrence probabilities of jet fire, explosion, and leakage accidents, respectively, associated with the leak size i. These formulations provide a basis for risk assessment by linking leak probability with ignition scenarios. They allow for evaluating the likelihood of fire and explosion accidents under different leak sizes.

2.3. Consequence prediction

The workflow for consequence prediction includes random variable sampling, CFD simulation, data processing, and consequence prediction using the Deep Neural Network-Long Short-Term Memory (DNN-LSTM) model.

Step 1: Credible leakage scenarios

A set of inputs for simulation is established by the LHS technique based on five random variables: leak rate, leak direction, leak location, wind speed, and wind direction. Their Probability Density Functions (PDFs) are first determined from a historical database and then divided into N intervals. Each sample (m_i) ensures that the area of each interval under the curve is equal. Thus, sampling results (x_i) can be obtained by:

$$x_i = F^{-1}\left(\frac{m_i - 0.5}{N}\right) \tag{5}$$

Step 2: Data processing

Random variables are sampled using the LHS technique and subsequently inputted into numerical simulation software STAR-CCM+. In total, 150 leakage scenarios (see Appendix A) are generated for critical leakage position prediction using the DNN model and time-series concentration prediction using the LSTM model. They are normalised using MinMaxScaler normalisation [39] to avoid the influence of scale differences by mapping a sampling value x_i between zero to one, i.e., $x_{i\text{-}normal}$.

$$x_{i-normal} = \frac{x_i - \min\{x_i\}}{\max\{x_i\} - \min\{x_i\}} \tag{6}$$

where $\min\{x_i\}$ and $\max\{x_i\}$ denote the minimum and maximum values of the variable x_i. Physically, Eq. (6) shifts the raw value relative to the minimum and then scales it proportionally to fit within the interval [0, 1]. As a result, the output needs to be anti-normalised to recover the original values $x_{i\text{-}return}$, which can be calculated by [44]:

$$x_{i-return} = x_{i-normal} \times (\max\{x_i\} - \min\{x_i\}) + \min\{x_i\} \tag{7}$$

Eq. (7) performs the inverse operation to rescale the normalised data back to its physical meaning. For example, the gas concentration at a monitoring point varies between 0 ppm and 10000 ppm. For

an value of 2500 ppm, based on Eq. (6), the normalised value is computed as $x_{i\text{-}normal}$=(2500-0)/(10000-0)=0.25.

Step 3: DNN-LSTM

Figure 3 presents the structure of the DNN-LSTM model. For the DNN model, the output, including concentration and corresponding location information, is divided into training (80%) and testing (20%) subsets, following the rules in [45]. A ReLU activation function is used in the DNN model (including input layer, hidden layers, and output layer) to predict the critical leakage position. The input layer requires the above normalized random variables, which are expanded through the first three hidden layers and compressed in the fourth hidden layer. The output concentrations at different leakage positions are predicted as [46]:

$$\begin{aligned} H^l &= \sigma(H^{l-1}W^l + b^l), \quad (1 < l < L) \\ O &= H^l W^{l+1} + b^{l+1} \end{aligned} \tag{8}$$

where the output H^l is controlled by the activation function σ, weight matrix W, and bias vector b. The procedure is applied to middle layers from 1 to l-1. The output layer O is controlled by the weights and activation functions. Parameters of the DNN model is summarised in Table 1. Four hyperparameters are optimised using grid search (see Figure 4), with Mean Squared Error (MSE) employed as the loss function to evaluate the average squared deviation between the true and predicted values [37].

$$MSE = \frac{1}{n}\sum_{i=1}^{n}\left(\hat{x}_i - x_i\right)^2 \tag{9}$$

where x_i is the true value of ith sample (e.g., gas concentration at a specific time and position); $\hat{x}_i$ is the corresponding predicted value generated by the DNN or LSTM model; n is the number of samples.

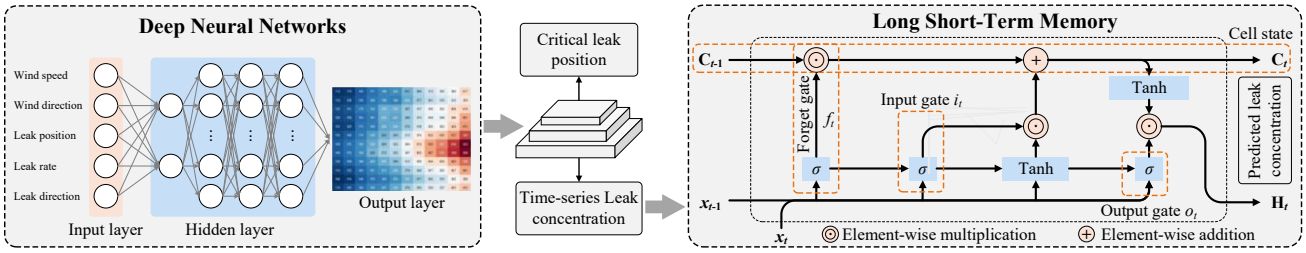

Figure 3. The structure of DNN-LSTM model.

Table 1. Parameter configuration of the DNN model.

Parameter	Specification	Parameter	Specification
Training set	120 samples	Hidden layer 2	64 neurons
Testing set	30 samples	Hidden layer 3	128 neurons
Input layer	wind speed; wind direction; leak rate; leak position; leak direction	Hidden layer 4	256 neurons
Output layer	concentration at 189 monitoring points	Hyperparameters	batch size: 40; learning rate: 1×10^{-3}; dropout rate: 0.1; epochs: 1000
Hidden layer 1	32 neurons		

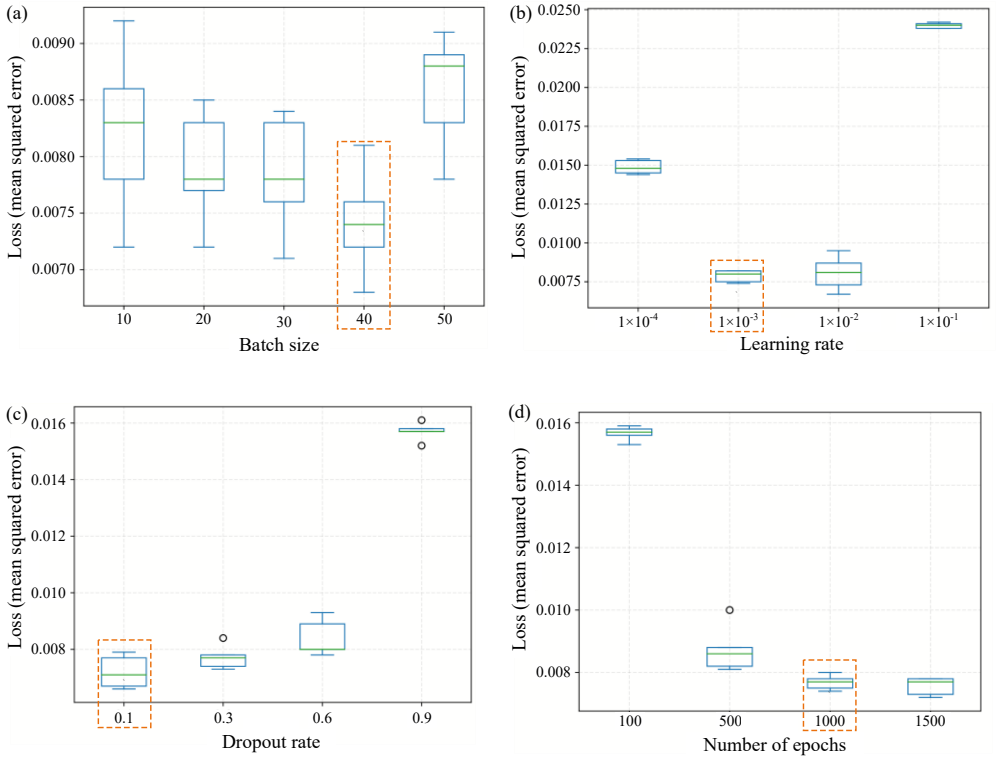

Figure 4. Comparison of error boxplots for different hyperparameter configurations of the DNN model: (a) batch size; (b) learning rate; (c) dropout rate; (d) number of epochs.

The time-series concentration x_t at critical leakage position is then input into the LSTM model. The information is added to the cell state c_t when the input gate is activated. The output vector (f_t, i_t, c_t, o_t) at each propagation step is controlled by the activation functions σ and *tanh*, weight W and H, and bias b. Detailed propagation behaviours can be expressed as [47]:

$$\begin{cases} i_t = \sigma(W_i x_t + U_t h_{t-1} + b_i) \\ f_t = \sigma(W_f x_t + U_f h_{t-1} + b_f) \\ o_t = \sigma(W_o x_t + U_o h_{t-1} + b_o) \\ \tilde{c}_t = \tanh(W_c x_t + U_c h_{t\text{-}1} + b_C) \\ c_t = f_t \square\ c_{t-1} + i_t \square\ \tilde{c}_t \\ h_t = o_t \square\ \tanh(c_t) \end{cases} \tag{10}$$

The definition of notations use in Eq. (10) is summarised in Table 2. Detailed parameter configuration of the LSTM model is summarised in Table 3. Four hyperparameters are optimised using grid search based on the criteria of MSE, as shown in Figure 5.

Table 2. Definition of notations used in Equation (10).

Parameters	Significance	Parameters	Significance
x_t	Current input	W	Input weight matrix
h_{t-1}, h_t	Previous and current hidden state	U	Hidden state weight matrix
c_{t-1}, c_t	Previous and updated cell state	b	Bias term
$\square$	Element-wise multiplication	σ	Sigmoid activation function
i_t, f_t, o_t	Input, forget, and output gate activations, respectively.		

Table 3. Parameter configuration of LSTM model.

Component	Specification	Component	Specification
Training set	120 samples	Hidden layer 2	64 neurons
Test set	30 samples	Hidden layer 3	128 neurons
Input layer	Concentration sequence of first 20 s	Hidden layer 4	256 neurons
Output layer	Concentration sequence of last 100 s	Hyperparameters	batch size: 64; sliding window size: 20;
Hidden layer 1	32 neurons		number of memory cells: 20; epochs: 200

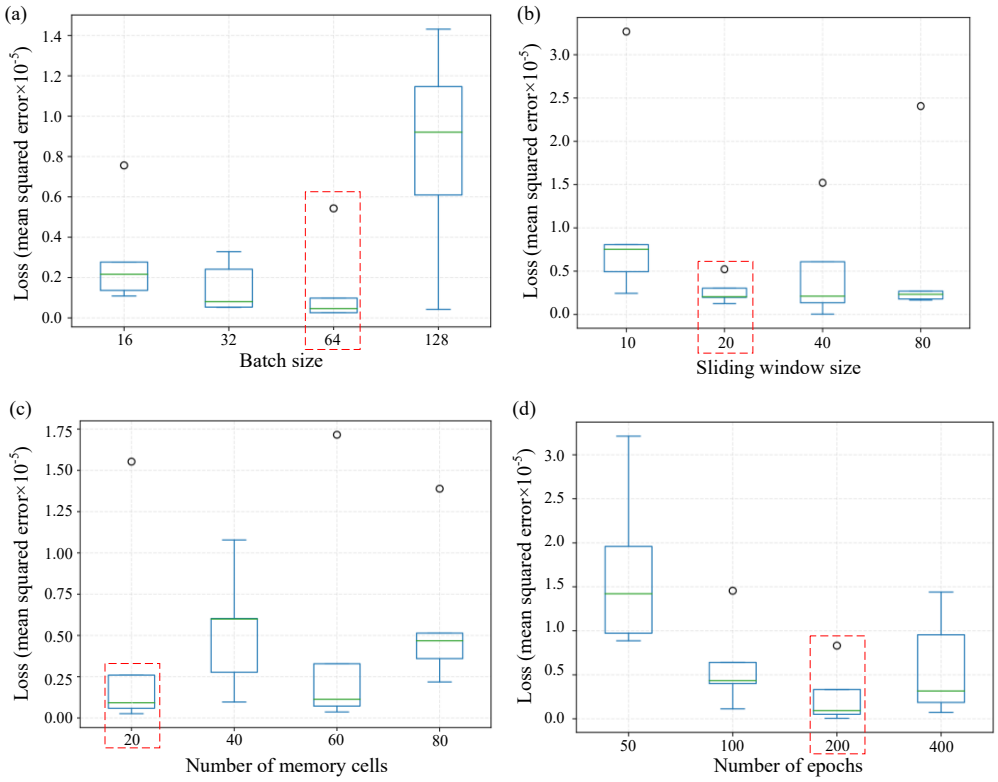

Figure 5. Comparison of error boxplots for different hyperparameter configurations of the LSTM model: (a) batch size; (b) sliding window size; (c) number of memory cells; (d) number of epochs.

The Mean Absolute Error (MAE), Root Mean Squared Error (RMSE), Correlation Coefficient (CC), and MSE are used to evaluate the performance of the model [34-37], as:

$$MAE = \frac{1}{n}\sum_{i=1}^{n}\left|\hat{x}_i - x_i\right| \tag{11}$$

$$RMSE = \sqrt{\frac{1}{n}\sum_{i=1}^{n}\left(\hat{x}_i - x_i\right)^2} \tag{12}$$

$$CC = \frac{\sum_{i=1}^{n}(\hat{x}_i - \bar{\hat{x}})(x_i - \bar{x})}{\sqrt{\sum_{i=1}^{n}(\hat{x}_i - \bar{\hat{x}})^2}\sqrt{\sum_{i=1}^{n}(x_i - \bar{x})^2}} \tag{13}$$

where $\bar{\hat{x}}$ is the mean of the predicted values, $\bar{x}$ is the mean of the actual values.

2.4. Risk analysis

The simulation software PHAST 8.22 is employed to simulate the consequences of fire and explosion accidents. The consequences are quantified as the fatality probability under heat radiation thresholds of 4 kW/m^2, 12.5 kW/m^{2,} and 37.5 kW/m^2 (for fire), or under overpressure thresholds of [0.2, 0.3], [0.3, 0.5], [0.5, 1], and [1, +∞] bar (for explosion). The consequence of the leak accident is quantified by the maximum concentration of flammable gas, expressed in units of parts per million (ppm). Accordingly, the risk corresponding to each leak size is calculated as:

$$R_i = \sum_i (C_i \times \mathrm{P}_i) \tag{14}$$

where C_i denotes the consequence of an accident (concentration for leaks, fatality probability for fire and explosion); P_i denotes the occurrence probability of the corresponding accident; i corresponds to leak sizes of 0.1%, 1%, 10%, and 100% of the flow cross-sectional area, respectively. For instance, the flow diameter is 100 mm, resulting in leak sizes of 0.1 mm, 1 mm, 10 mm, and 100 mm. Based on Eq. (14), the unit of risk is expressed in ppm for leakage accidents and in percentages for fire and explosion accidents.

3. Case study

3.1. System description and critical component identification

Hydrogen production from offshore wind provides a promising solution for offshore energy development, including energy production (electricity generation), transformation (electricity to preservable hydrogen), transportation (pipes and vessels), and consumption (hydrogen industry onshore). Among these processes, hydrogen storage supported by an offshore hydrogen storage system plays a critical role in offshore hydrogen transformation and transportation. However, harsh offshore conditions, such as salt spray and microbial activity, may cause structural pitting corrosion and accelerate degradation of hydrogen storage structures. These damages can be further aggravated by the wind-wave coupling loads and collisions, therefore increasing the component failure probability [48]. In this study, these effects are modelled as failure probability with different leak sizes for predictive risk analysis of offshore hydrogen storage systems.

The offshore hydrogen storage system consists of four subsystems: control and monitoring, automated control, storage and delivery, and preparation, see Table 4. The control and monitoring subsystem provides real-time data and early warnings; The automated control subsystem performs operational logic for safe regulation; The storage and delivery subsystem accommodates hydrogen under designed conditions and ensures reliable supply; The preparation subsystem performs compression, cooling, purification, and drying to guarantee the hydrogen quality. The RPNs of each component are summarised in Table 5 using the FMEA method. The result indicates that the storage tanks have the highest RPN, therefore, it is prioritised for the risk analysis.

Table 4. Main components of offshore hydrogen storage system.

Subsystems	Components
Control and Monitoring (CM)	Magnetic Float Level Gauge (MG), Flowmeter (FM), Pressure Sensor (PS), Temperature sensor (TS), Pipeline Level Indicator (PI), Pneumatic Ball Valve (PB), Control Valve (CV), Filling Pump (FP)
Automated Control (AC)	Programmable Logic Controller (PL), Industrial control computer (IC)
Storage and Delivery (SD)	Storage Tank (ST), Storage tank flange seal (SF), Warehouse Storage Tank (WT), Tower Storage Tank (TT)
Preparation (LP)	Filling Signal Station (FS), Fuel Transfer Valve (FV), Safety Overflow Valve (SV), Junction (JC), Gauge (RG)

Table 5. The RPNs of components of offshore hydrogen storage system.

Components	S	O	D	RPN×10^{-2}	Components	S	O	D	RPN×10^{-2}
MG	0.58	0.32	0.26	5.00	**ST**	**2.15**	**0.58**	**0.59**	**74.29**
FM	0.88	0.50	0.37	16.80	SF	0.63	0.42	0.21	5.85
CV	0.19	0.14	0.14	0.40	WT	1.44	0.19	0.15	4.51
PB	1.43	0.78	0.60	68.85	TT	1.65	0.12	0.14	3.10
PS	0.52	0.22	0.14	1.70	FS	0.55	0.12	0.07	0.47
TS	0.49	0.15	0.18	1.46	FV	0.55	0.27	0.19	2.86
PI	0.37	0.16	0.15	0.94	SV	0.33	0.20	0.12	0.84
FP	1.29	0.97	0.53	67.82	JC	0.55	0.22	0.17	2.12
PL	0.63	0.32	0.11	2.27	RG	1.25	0.77	0.42	41.36
IC	0.39	0.32	0.10	1.36					

3.2. Data sources

To avoid additional uncertainty from distributional assumptions, the discretisation method [49] is applied to model the PDFs of the five input variables, including wind speed, wind direction, leak rate, leak position, and leak direction. Specifically, the collected data are divided into several intervals, and the frequency of occurrence in each interval is counted. The probability of each interval is calculated as the ratio of the corresponding frequency to the interval width. The wind speed and wind direction data are collected from a real offshore wind farm [50]. The leak position is divided into six intervals with leakage accidents based on the spatial discretisation method, see Figure 6. The leak direction is averaged into six directions (±X, ±Y, and ±Z). The leak rate is collected from the HyRAM database [16] and divided into three ranges: 0-1 kg/s, 1-10 kg/s, and 10-20.8 kg/s. The statistical information of the five input variables is summarised in Table 6, Table 7, Table 8. Finally, 150 leakage scenarios are sampled by the LHS technique, as detailed in Appendix A.

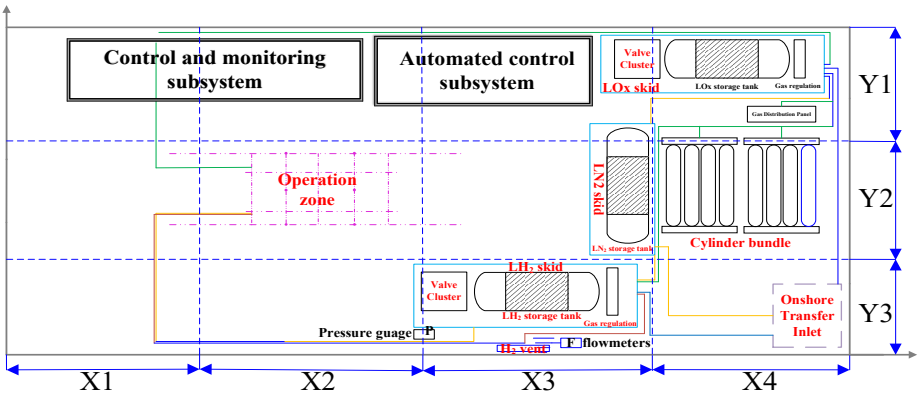

Figure 6. Spatial discretization of offshore hydrogen storage system.

Table 6. Statistic information of leak position, leak direction, and leak rate.

Leak position (Interval index)	Probability	Leak direction (Interval index)	Probability	Leak rate (Interval index)	Probability
X4Y1 (0-1)	0.2823	+X (0-1)	1/6	0.1-1.0 (0-1)	0.7281
X4Y2 (1-2)	0.2721	-X (1-2)	1/6	1.0-10.0 (1-2)	0.2435
X3Y1 (2-3)	0.1447	+Y (2-3)	1/6	10.0-20.8 (2-3)	0.0284
X4Y3 (3-4)	0.1443	-Y (3-4)	1/6		
X1Y2 (4-5)	0.1407	+Z (4-5)	1/6		
X3Y3 (5-6)	0.0158	-Z (5-6)	1/6		

346 Table 7. Statistic information of wind speed.

Wind speed (m/s)	Probability	Wind speed (m/s)	Probability	Wind speed (m/s)	Probability
0-1	0.0071	7-8	0.0931	14-15	0.0346
1-2	0.0221	8-9	0.0951	15-16	0.0256
2-3	0.0396	9-10	0.0905	16-17	0.0188
3-4	0.0549	10-11	0.0802	17-18	0.0128
4-5	0.0679	11-12	0.0685	18-19	0.0087
5-6	0.0817	12-13	0.0562	19-20	0.0058
6-7	0.0901	13-14	0.0457		

347

348 Table 8. Statistic information of wind direction.

Wind direction (°)	Probability	Wind direction (°)	Probability	Wind speed (m/s)	Probability
0-45	0.0563	135-180	0.1971	270-315	0.0915
45-90	0.1126	180-225	0.1901	315-360	0.0352
90-135	0.1690	225-270	0.1478		

349

350 The Empirical Cumulative Distribution Function (ECDF) of the sampled data is compared with
351 Cumulative Distribution Function (CDF) of original variables to compute the maximum deviation D
352 among them. A smaller D value indicates a lower level of uncertainty. Additionally, the 95%
353 confidence bounds of Kolmogorov-Smirnov (K-S) static is used to evaluate whether the ECDF falls
354 within the acceptable range of the CDF. Both the K–S statistic and the associated p-value are computed
355 to assess the goodness of fit and thereby measure the uncertainty. Figure 7 illustrates the uncertainty
356 quantification for five variables, namely wind speed, wind direction, leak position, leak direction, and
357 leak rate. The results confirm that the LHS technique can reliably reproduce the target distributions of
358 input variables [51].

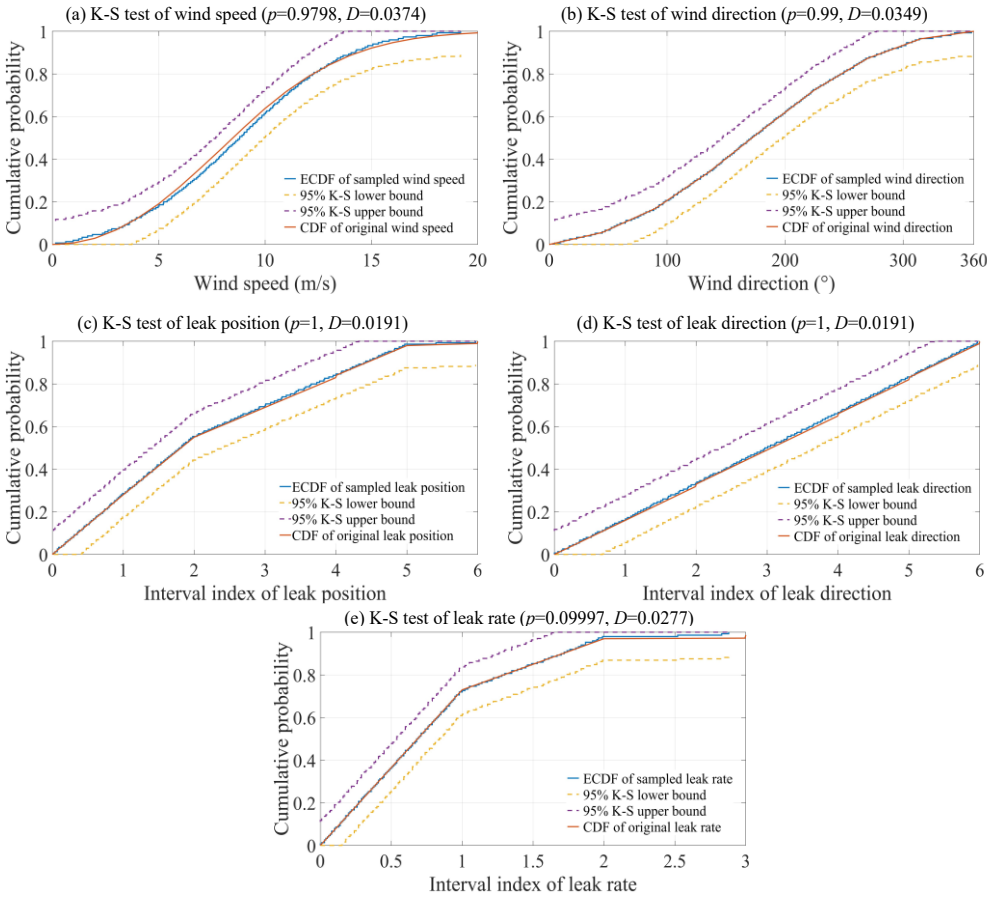

Figure 7. Uncertainty quantification of five sampled variables: (a) wind speed; (b) wind direction; (c) leak position; (d) leak direction; (e) leak rate.

3.3. Model construction and verification

Hydrogen storage tank (suggested by FMEA) is selected as a case to illustrate the applicability and effectiveness of the proposed method. The offshore hydrogen storage system is modelled based on a real-word design, as shown in Figure 8. The incompressible ideal gas law, pressure-based solver, standard k-ε model, non-homogeneous equilibrium model, and Lee's model [52] are applied to characterize flows in leakage accidents. Since hydrogen approaches a steady state in terms of leak position and concentration at approximately 120 seconds, the simulation time is set to 120 seconds.

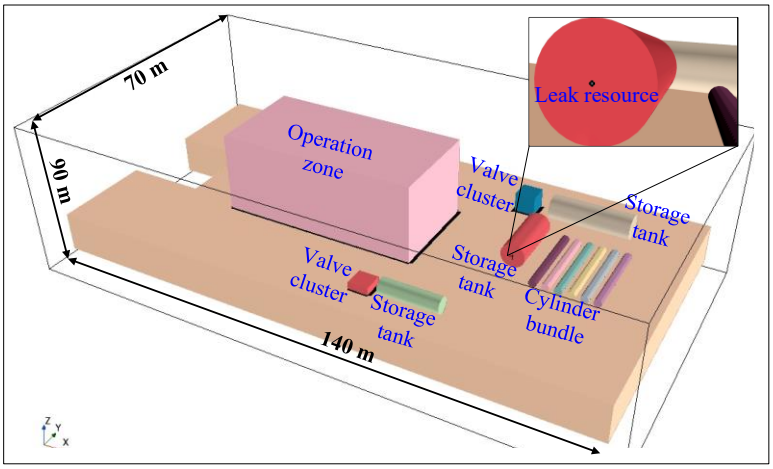

Figure 8. Simulation model for offshore hydrogen storage platform.

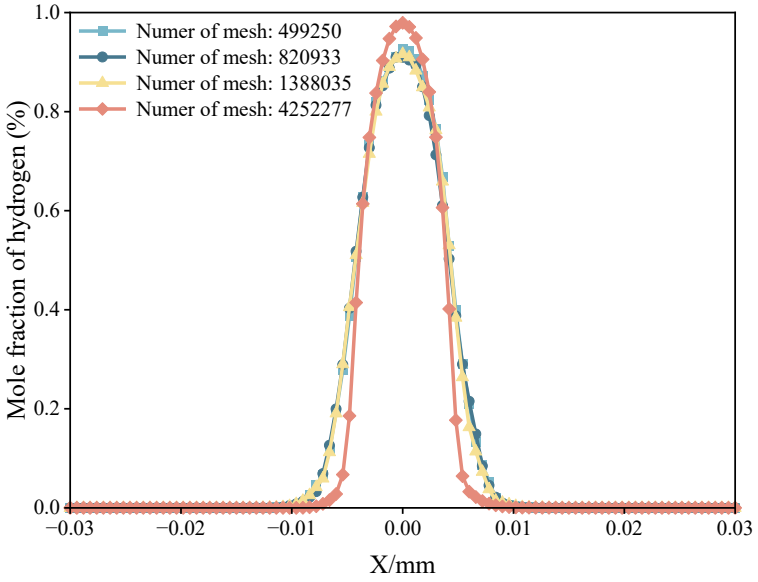

Figure 9. Sensitivity analysis of simulation results to mesh quality.

A well-documented hydrogen leak experiment from [53] is used to verify the feasibility of the established hydrogen leakage model. Notably, due to no available experimental is identical to the presented case model, the similar hydrogen leak experiment designed by Houf et al. [53] is adopted as a benchmark, which have been widely employed for validating hydrogen leakage [45]. The experimental apparatus, as shown in Figure 10(a), consisted of a 1.91 mm hydrogen nozzle and a 63.50 mm air co-flow tube. The flow rate of hydrogen is controlled by calibrated mass-flow controller. The operating condition is maintained at ambient temperature (21±1 °C) and pressure (100±5 kPa). The

hydrogen exit velocity is set as 134 m/s, corresponding to a Reynolds number of 2384. As a result, a numerical model with a computational domain of 250 mm × 250 mm × 190 mm is constructed to reproduce the experimental configuration, as shown in Figure 10(b). The boundary continual and model setting match those described above.

The simulated mole fraction of hydrogen is compared with the experimental measurements at axial planes (Z=10, 25, 50, 75, 100 mm), as shown in Figure 10 (c) and (d). The numerical model captures the centreline peak and the radial decay of the plume at all planes, as well as the increase in plume width with axial distance, indicating promising agreement with the experiments. Minor deviations close to the nozzle are attributed to idealised inlet conditions and measurement uncertainty, but they do not affect the conclusions regarding the dynamic behaviour of hydrogen leakage. Overall, the numerical model is able to reflect the dynamic behaviour of hydrogen leakage and dispersion.

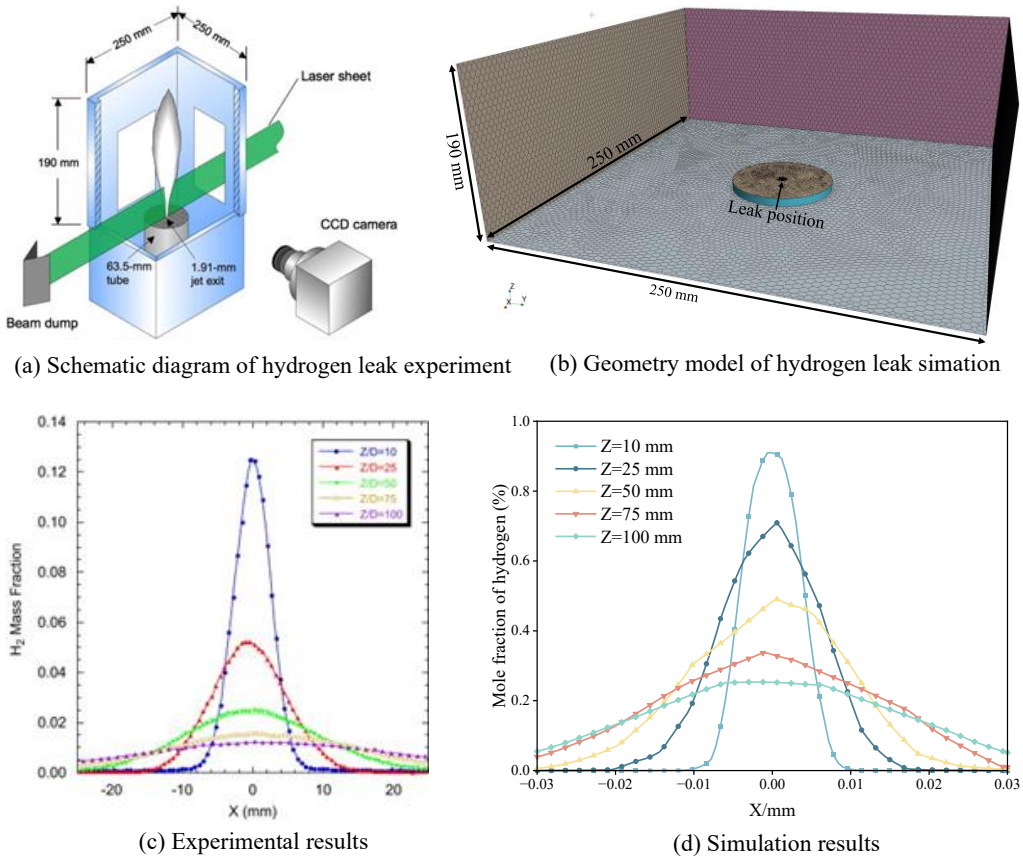

(a) Schematic diagram of hydrogen leak experiment (b) Geometry model of hydrogen leak simation

(c) Experimental results (d) Simulation results

Figure 10. Experimental layout and model validation: (a) schematic of the hydrogen leak experiment [53]; (b) numerical model; (c) experimental mole-fraction profiles of hydrogen; (d) simulated mole-fraction profiles of hydrogen.

Figure 11 presents the results of numerical simulation for six hydrogen leak scenarios. A region of high gas concentration forms near the leakage source due to the pressure difference between the interior and exterior environments. Wind speed also plays a critical role in shaping the diffusion behaviour of released hydrogen. Increasing wind speed enhances local turbulence intensity, causing grater diffusion range and more rapid mix with air, as in [30]. Similarly, the leak rate significantly influences the hydrogen diffusion when the wind energy is insufficient to overcome the energy of the leak flow. A numerical simulation in [36] demonstrates the effects of wind speed and leak rate. Additionally, structural components or obstacles within the system further hinder the uniform distribution of hydrogen, creating localized concentration anomalies. The associated risks are increased under specific conditions: (i) when the structural components are sensitive to hydrogen embrittlement and an ignition source is present, (ii) when high-speed winds align with the direction of the leak, exacerbating the spread of hydrogen, and (iii) when the leakage accidents occur in the limited space, complicating safety management and emergency response. Although numerical simulations effectively capture these complex relationships, the extensive computational time required poses a significant challenge to predictive risk assessment. To address this, the DNN-LSTM model is a robust option for capturing and predicting these relationships between inputs and outputs, providing insights into potential future changes in accident risks.

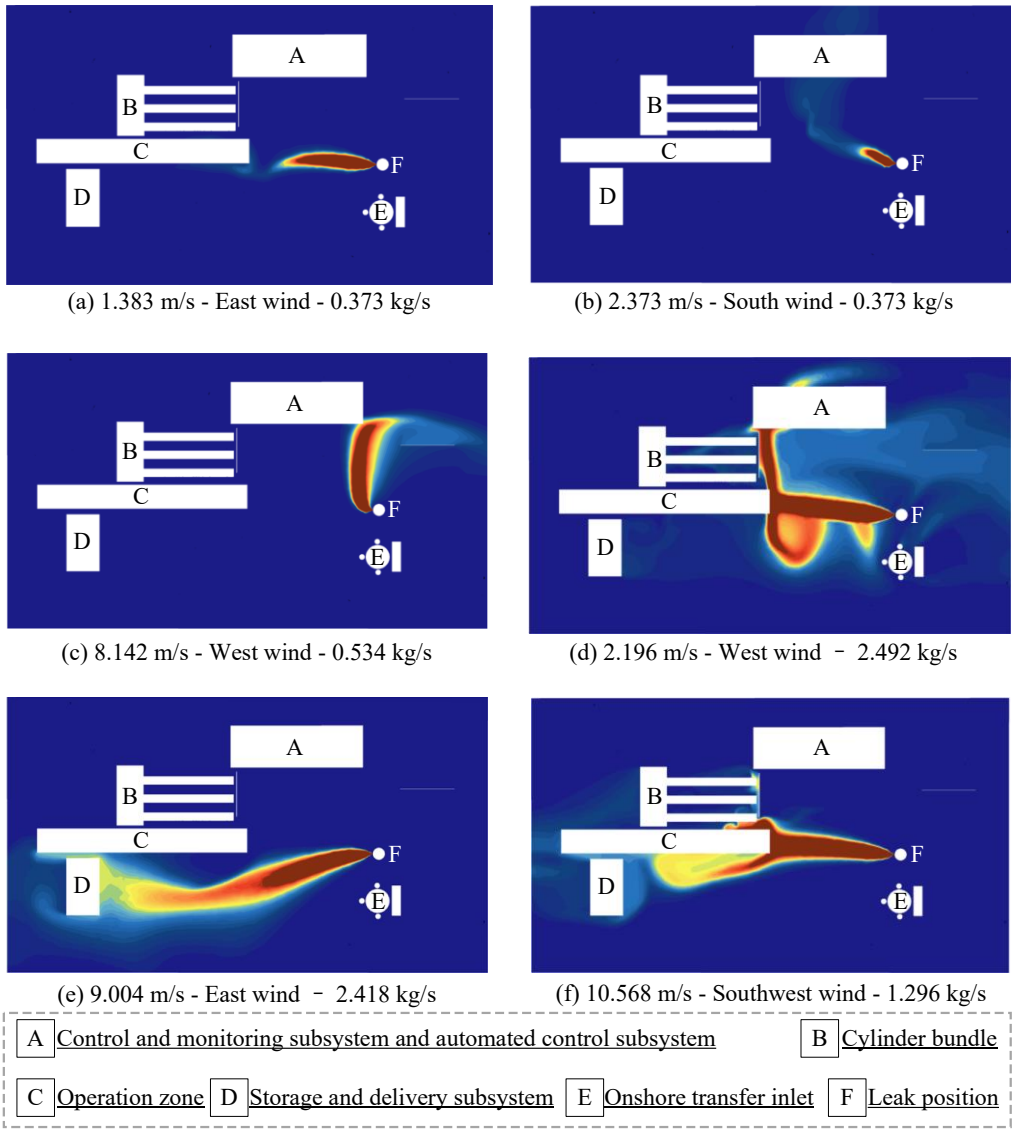

Figure 11. Results of numerical simulation for hydrogen leakage scenarios.

3.4. Probability estimation

(1) Leakage probability

The leak probability estimation model is expressed a function of leak size, as shown in Figure 12(a). The input information based on non-parametric approach is summarized in Table 9 according to the database that reported in [20] and [54].

Table 9 Input of hierarchical Bayesian model.

Parameter	Information	parameter	Information
Prior α_1	$\alpha_1 \sim N(\alpha_{11}, \alpha_{12})$	Hyperprior α_{12}	$\alpha_{12} \sim U(0, 1\times10^{3})$
Prior α_2	$\alpha_2 \sim N(\alpha_{21}, \alpha_{22})$	Hyperprior α_{21}	$\alpha_{21} \sim N(0, 1\times10^{-3})$
Prior τ	$\tau \sim$ Gamma (1, 5)	Hyperprior α_{22}	$\alpha_{22} \sim U(0, 1\times10^{3})$
Model	$\log(\mu_{LP}) = \alpha_1+\alpha_2 \log(LA)$	Likelihood LP	$LP \sim N(\mu_{LP}, \tau)$
Hyperprior α_{11}	$\alpha_{11} \sim N(0, 1\times10^{-3})$		

Figure 12(b) indicates that a linear relationship is observed between the leak probability and leak size. The leak probability decreases with increased leak size, indicating that smaller leak sizes are more likely to leak. This trend is consistent with risk-informed separation model. It reported that pinhole leaks dominate event counts whereas large breaches are rare but easier to observe, leading to lower estimation uncertainty [19-25].

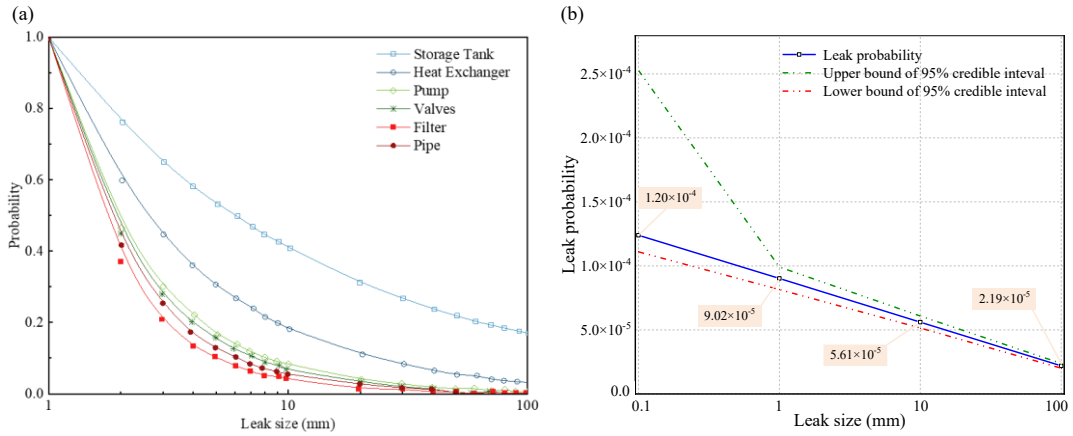

Figure 12. Leak probability estimation for storage tank.

A nonlinear model is established to assess the robustness of the estimation model, as [55]:

$$\log(\mu_{LP}) = \alpha_1 + \alpha_2 \log(LA) + \alpha_3[\log(LA)]^2 \quad (15)$$

This model employs a non-informative prior distribution for α_3, defined as $\alpha_3 \sim N(0, 1\times10^{-3})$, which represents a normal distribution with a mean of zero and a very small variance (1×10^{-3}). It can minimize assumptions about the value parameter α_3, ensuring that the model relies primarily on the observed

data to guide the estimation process. Figure 13 displays the 95% confidence interval of α_3 for each component. The original model fits most components except the pumps and valves. This is because of the scarcity of 1% and 0.1% leak size from generic databases. The estimation of the pipe has the greatest uncertainty due to great variability in the database or few available data.

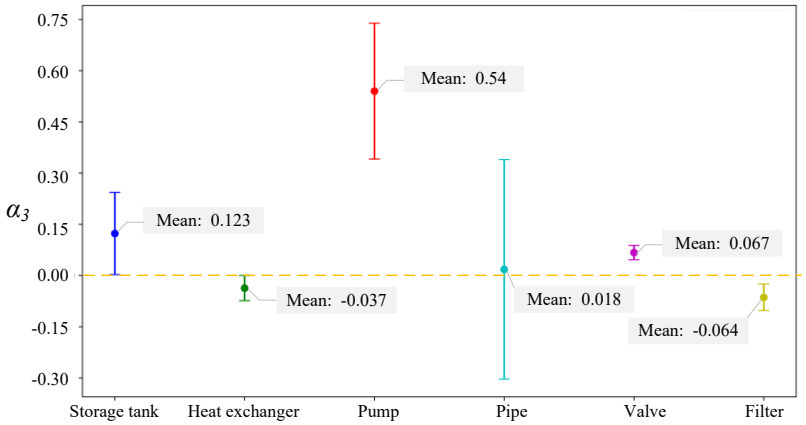

Figure 13. Confident interval (95%) of the posterior distributions of components.

(2) Fire and explosion probabilities

The leak detector has a failure rate of 0.64, and the shutoff valve has a failure rate of 0.1 [25]. The ignition type is classified as immediate or delayed ignition according to the ignition time. The former occurs within 0.1 seconds after leakage, and the latter occurs within 5 seconds after leakage. The immediate ignition probability ($P_{imm.ign}$) derives from [25] and the delay ignition probability ($P_{delay.ign}$) is calculated by:

$$P_{delay.ign} = 1 - P_{imm,ign} \tag{16}$$

Figure 14 shows the event tree where leakage is an initial accident. Table 10 summarizes the probabilities of fires and explosions with different leak sizes. The probability of explosion is greater than that of jet fire due to the higher probability of delayed ignition.

Table 10. Probability of fires and explosions

Type of accident	Leak size			
	Minor	Medium	Major	Rupture
Jet fire	2.40×10^{-6}	1.80×10^{-6}	1.12×10^{-6}	4.38×10^{-7}
Explosion	9.60×10^{-6}	7.22×10^{-6}	4.49×10^{-6}	1.75×10^{-6}

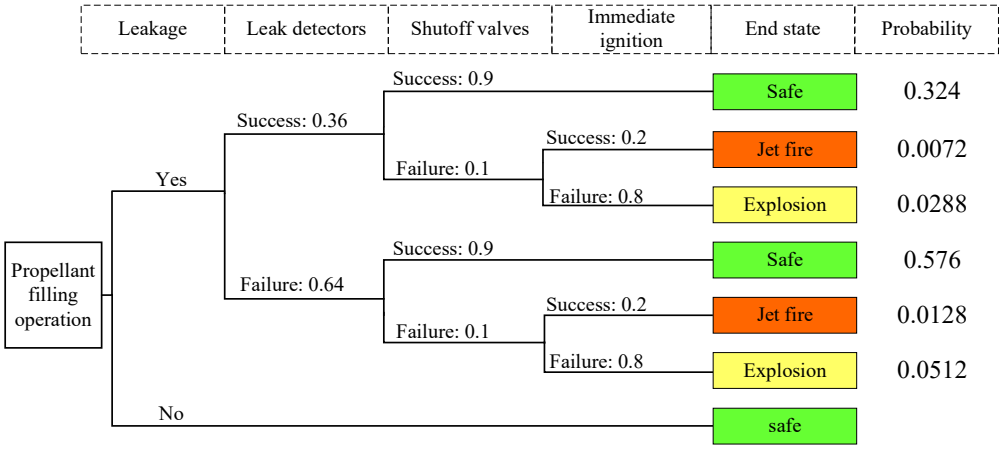

Figure 14. Event tree for the scenario of liquid hydrogen leakage from storage tanks.

3.5. Consequence prediction

Figure 15(a) presents the predictions of critical leakage position by the DNN model. Green dashed box ① denotes the comparison of high-concentration region between the true and predicted values; ② denotes the comparison of low-concentration region between the true and predicted values. The DNN model demonstrates prediction performance for the true simulation results in box ②, particularly when leakage concentration is relatively low. However, in box ①, the DNN model is used only to predict the critical leakage position rather than to predict the full concentration field and it is sufficient for this purpose [47]. In Figure 15(b), the concentration concentrated within approximately 5 m and then dispersed to a distance of nearly 90 m under the influence of environmental factors. The observed variability in leakage positions supports the necessity of applying the DNN model to identify critical leak locations.

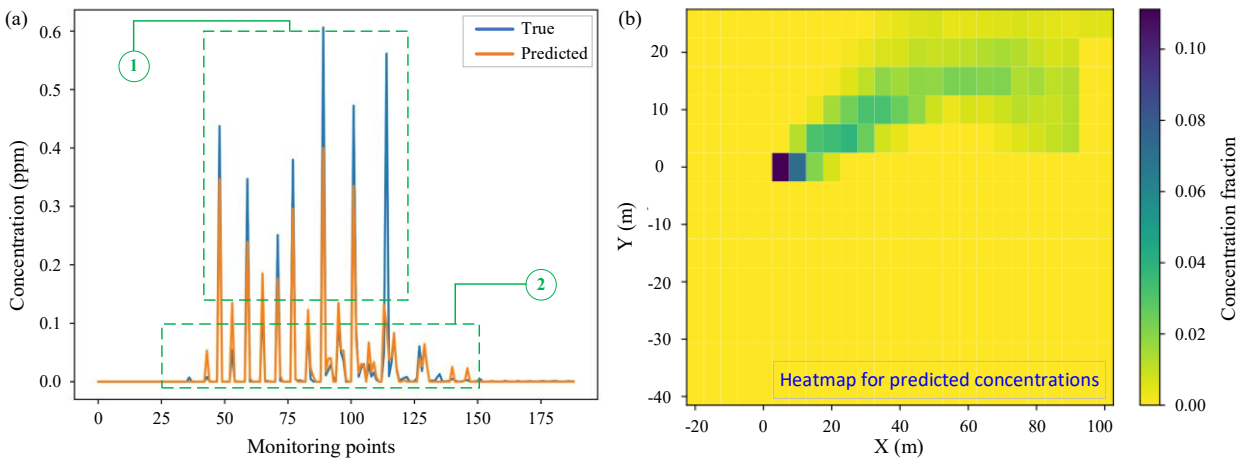

Figure 15. Prediction of critical leakage position by the DNN model.

Figure 16 shows the predictions of time-consequence from critical leakage position by the LSTM model. Overall, the LSTM model accurately predicts time-series concentration. Importantly, the leakage concentration shows significant dynamic developmental behaviour rather than remaining at a fixed value, highlighting the need for a dynamic perspective when assessing leakage risks.

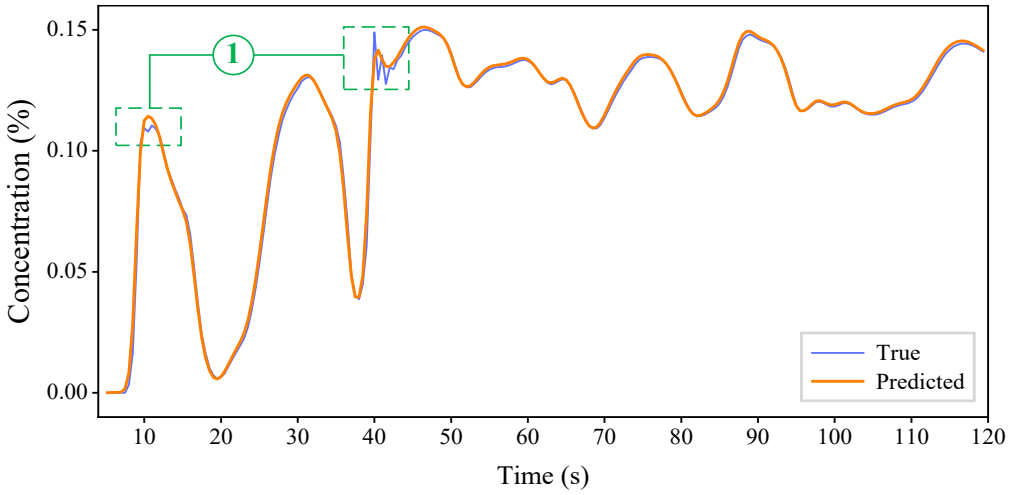

Figure 16. Prediction of time-series consequence by LSTM.

Baseline models, including back propagation (BP), polynomial regression (PR), and artificial neural network (ANN), recurrent neural network (RNN), gate recurrent unit (GRU), and autoregressive model

493 (AR), are compared with the proposed DNN-LSTM model in Table 11. The result indicates that the
494 DNN-LSTM model achieves the minimum output loss among all methods.
495
496 Table 11 Comparisons of MLAs

Model	MSE	MAE	RMSE	CC
BP	0.03	0.19	2.35	0.77
RP	3.05×10^{-3}	2.13×10^{-2}	1.96	0.90
ANN	7.59×10^{-4}	5.32×10^{-3}	0.98	0.89
DNN	$\mathbf{1.10\times10^{-5}}$	$\mathbf{7.73\times10^{-4}}$	**0.01**	**0.99**
RNN	8.56×10^{-5}	4.91×10^{-2}	0.321	0.763
GRU	5.23×10^{-5}	2.53×10^{-2}	0.037	0.854
AR	6.71×10^{-5}	2.50×10^{-2}	0.562	0.766
LSTM	$\mathbf{2.89\times10^{-6}}$	$\mathbf{1.08\times10^{-3}}$	**0.010**	**0.992**

497

498 ## 3.6. Risk analysis

499 **(1) Time-series leakage risk**

500 According to [19] and [56], hydrogen concentration thresholds are classified and adopted to assess the
501 time-series leakage risks, including [0, 4×10^4], [4×10^4, 6.7×10^4], [6.7×10^4, 7.5×10^4], and [7.5×10^4,
502 10×10^4] ppm. Since leak probability is strongly dependent on the leak size, the risk thresholds
503 associated with leak sizes are determined by multiplying the concentration threshold with the leak
504 probability of corresponding leak size, see Table 12.

505 Table 12 Risk level under different leak sizes.

Leak accident	Probability	Risk threshold (ppm)			
		Level 1	Level 2	Level 3	Level 4
0.01 mm leaks	1.20×10^{-4}	4.80	8.04	90.00	120.0
1 mm leaks	9.02×10^{-5}	3.61	6.04	67.70	90.21
10 mm leaks	5.61×10^{-5}	2.24	3.76	42.10	56.10
100 mm leaks	2.19×10^{-5}	0.876	1.47	16.40	21.90

506

507 Figure 17 presents the time-series risk analysis results for different leak sizes, which confirm that 0.1
508 mm and 1 mm leaks hold less hazardous and do not cause fires and explosions, but leakage risk varies

over time, suggesting that a fixed risk value cannot reflect the complexity and variability of the actual situation. Moreover, acceptable risk criteria specific to the offshore hydrogen storage system are obtained by comparing other acceptable risk criteria. Figure 18 shows the individual risks at axial distances from the leakage source. The acceptable risk criteria have a significant impact on hazardous zones, and it is determined to be 10^{-6} per year [46].

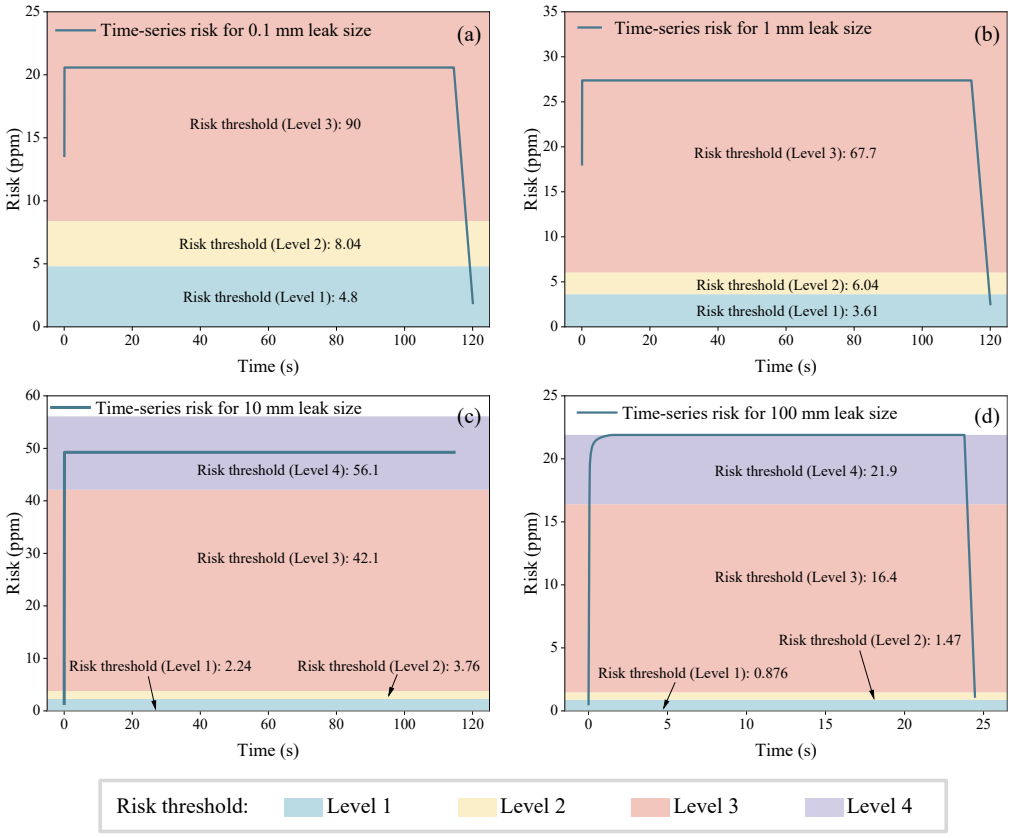

Figure 17. Time-series risk of leaks associated with leak sizes.

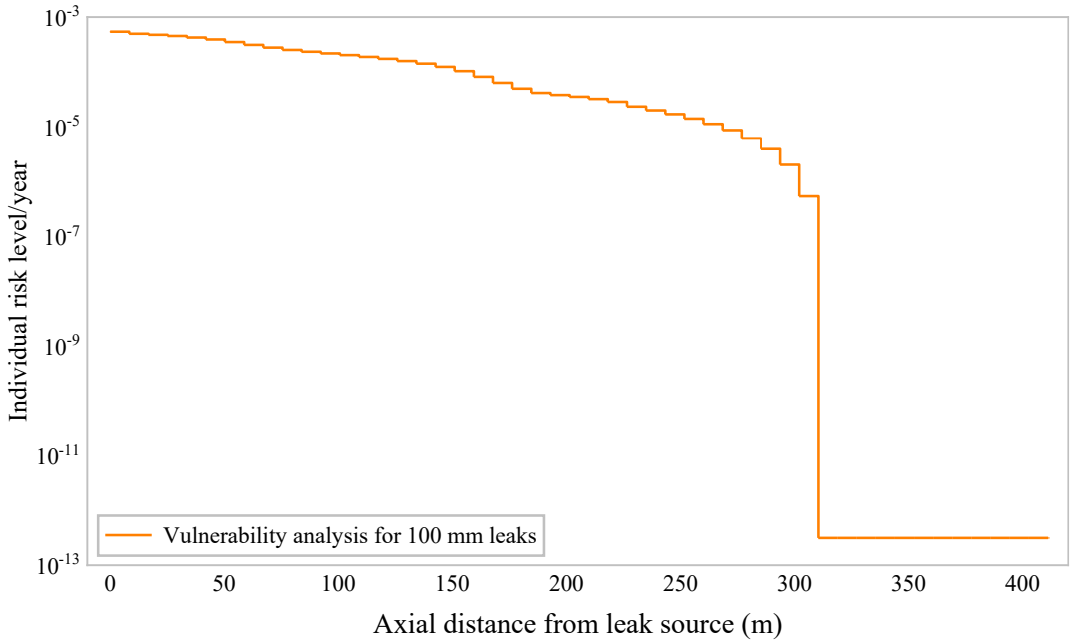

Figure 18. Risk level for 100 mm leaks under different acceptable risk criteria.

(2) Fire and explosion risks

Table 13 presents the results of risk analysis for fire and explosion, indicating that the leak accidents with a size below 0.1 mm generate negligible release and are unlikely to result in explosion accidents. The maximum hazardous zones of fire and explosion are under 1 m as the open space when leak size is less than 1 mm, indicating negligible damage. In contrast, larger damage zones are observed when the leak size exceeds 1 mm. It worth to noting that no potential correlation exists between risk probability and accident consequences. Furthermore, the explosion consequences remain consistent across leak sizes, since their peak overpressures are only associated with the leaking material.

Table 13 Results of fire and explosion risk assessment under different leak sizes.

Type of accident	Leak size (mm)	Probability	Consequence (mortality)	Risk	Maximum hazard distance (m)
Jet fire	0.1	2.40×10^{-6}	0.61%	1.46×10^{-8}	0.29
	1	1.80×10^{-6}	2.08%	3.75×10^{-8}	0.97
	10	1.12×10^{-6}	3.88%	4.35×10^{-8}	17.99
	100	4.38×10^{-7}	6.01%	2.63×10^{-8}	135.44
Explosion	0.1	9.60×10^{-6}	—	—	—
	1	7.22×10^{-6}			
	10	4.49×10^{-6}	23.05%	1.03×10^{-6}	41.13
	100	1.75×10^{-6}		4.03×10^{-7}	238.70

(3) Hazardous zone definition

Figure 19 shows the hazardous zone associated with leak sizes based on defined risk acceptable criteria. The result shows no concerns about damage for the leakage accident with less than 0.1 mm leak size. The main contributor of damage is the heat radiation of 12.5 kW/m² for 1 mm, 10 mm, and 100 mm leakage accidents. The leakage accident with 1 mm leak size is recognized as a low-risk due to low heat radiation. The result also indicates that the individual risk from 1 mm and 10 mm leakage accidents never exceeds 10^{-4} per year. However, the individual risk from 100 mm leakage accidents exceeds 10^{-4} per year.

The warning signals for three leakage accidents are summarised in Table 14. System operating variables, including pressure, mass flow rate, and leakage concentration, are used as warning indicators to approximate leak sizes. Accordingly, hazardous zones and corresponding preventive measures can be determined as follows.

- Low risk: Characterised by a slight concentration rise (e.g., from 0 ppm to 500 ppm), a minor pressure drops (e.g., from 101 kPa to 100.8 kPa), and small flow rate fluctuations. To prevent escalation, sensor consistency should be verified and targeted concentration inspections should be conducted near pipe joints. Activities should be restricted within a 5 m radius. The potential ignition sources should be controlled.
- Medium risk: Characterised by a significant concentration rise (e.g., reaching 5000 ppm or higher), a significant pressure drops (e.g., from 101 to 98 kPa), and a significant flow rate change. This level triggers active mitigation within a 25 m region, including isolating the suspected segment and reducing operating load.
- High risk. Characterised by a rapid surge in concentration, a sharp pressure drop and pronounced flow rate change. All activities should be stopped, followed by rapid isolation and pressure control. Personnel must be evacuated within a 200 m radius.

Table 14 Hazardous zones of different hazard responses.

Response Level	Corresponding leak size (mm)	Hazard distance (m)
Low	0.1 - 1	5
Medium	1 - 10	25
High	10 - 100	200

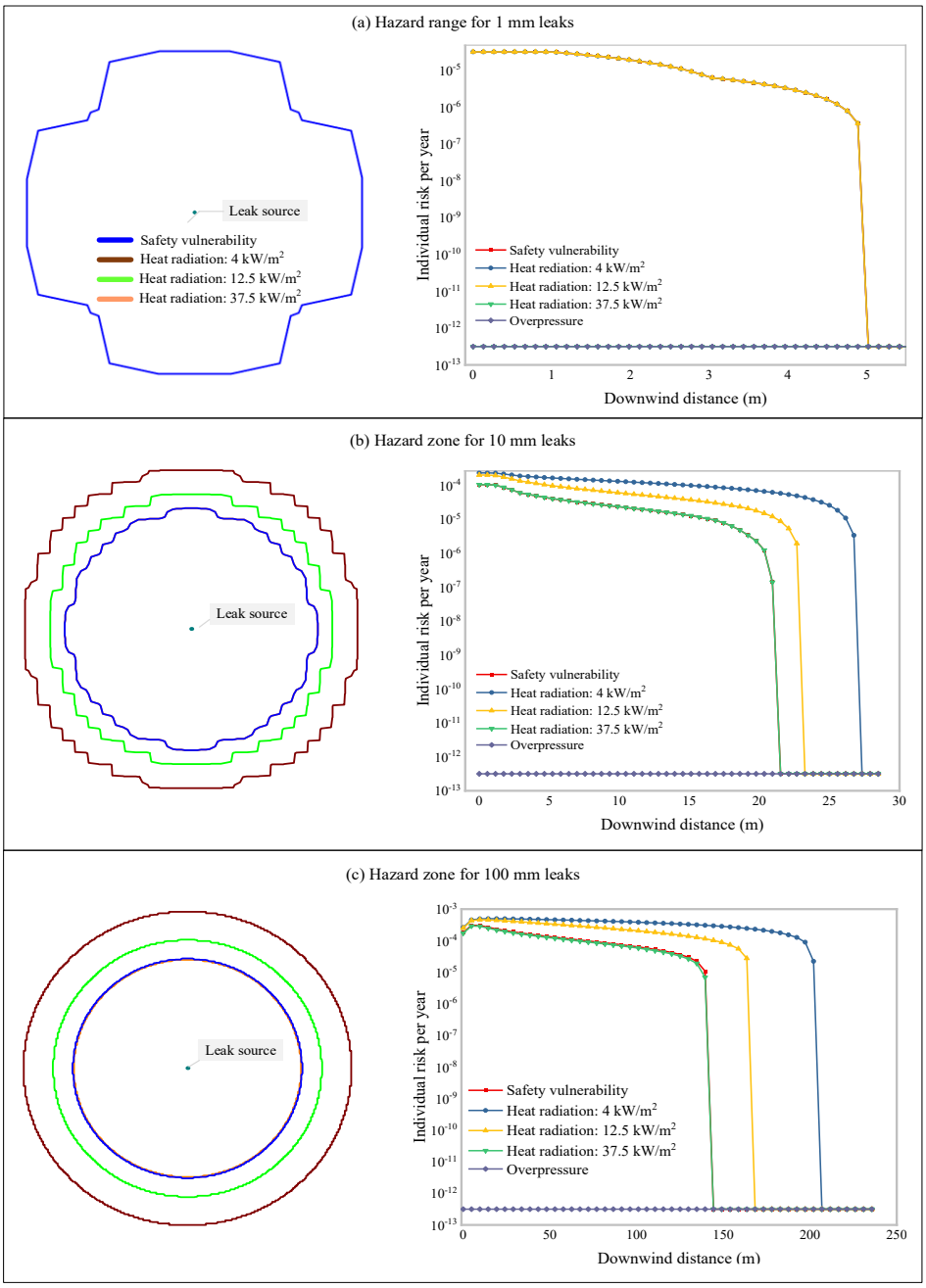

Figure 19. Hazardous zones for different leak sizes.

3.7. Discussions

Overall, this paper proposes a predictive risk analysis method that accounts for the dynamic nature of risks and enables real-time updates. The approach integrates hierarchical Bayesian failure estimation with time-series consequence analysis. Specifically, the occurrence probability of risk factors is estimated using a hierarchical Bayesian model, while the time-series consequences prior to accidents are predicted by a dynamic consequence model. The predictive framework significantly enhances the

ability to identify potential risks in advance and to implement preventive measures, thereby reducing the probability and severity of accidents. It is appliable not only in the design stage, but throughout its lifetime.

From the failure probability modelling perspective, the proposed method implicitly accounts for the offshore environmental effects using the estimated component failure probability associated with different leakage sizes. This formulation can be further refined by the offshore specific risk modification factors. As reported in [57], marine environment correction factor related to salt spray can be incorporated to modify component failure probability. Structural numerical simulations provide alternatives to link the vessel collision scenarios with failure probability models, to improve the reliability of risk assessment results [58]. In addition, most spectral fatigue models have been developed to assess the structural fatigue life, which can be used as evidence to support risk assessment of offshore system under wind-wave coupled conditions [59].

From the dynamic perspective, this study predicts the spatiotemporal evolution of hydrogen leakage concentrations using the DNN-LSTM model. Future work will extend the framework to time-dependent degradation modelling of component performance (e.g. cumulative hydrogen embrittlement), to link the component failure probability to cumulative damage mechanisms and therefore enable a more generalisable dynamic risk assessment framework.

From the leakage consequence perspective, the proposed DNN-LSTM model is trained as a surrogate of dispersion simulations. According to the diffusion mechanisms of hydrogen, the predicted leakage behaviour accurately represents (i) high-concentration position regions near the leak source [47], (ii) dynamic development behaviour of hydrogen concentration field, (iii) enhanced turbulent mixing mechanisms under varying environmental conditions [24,29], and (iv) localised concentration anomalies induced by obstacles [25]. Despite these advantages, the artificial intelligent-driven models may struggle to capture extreme concentration peaks and fine-scale turbulent fluctuations, as demonstrated in Figures 15 and 16. Moreover, the complex nonlinear networks reduce the interpretability of predictions. Therefore, future work will incorporate physical mechanisms into training process to enable interpretable and reliable risk predictions. Models include physics-informed

neural networks [60] and conservation-constrained models [61], which embed the specific diffusion models and/or hard constraints to improve physical consistency and to provide informative predictions.

4. Conclusions

A predictive risk analysis framework for capturing the dynamic development nature of leak accidents is proposed in this paper. According to the occurrence probability of risk factors and time-series consequences of events, the dynamic leak risk and hazardous zone are analysed. Meantime, a hazard response mechanism is developed to reduce the difficulty of detecting leak size. The feasibility of the proposed approach is validated by a comprehensive risk analysis of a real offshore hydrogen storage system. The results indicate that the greatest hazardous zone for 100 mm leaks is determined as 200 m, followed by 10 mm leaks (25 m) and 1 mm leaks (5 m). The results also indicate that the time-series risks of leakage accidents provide a dynamic and refined improvement over existing risk analysis approaches. Specifically, (i) it adapts to changing external factors by a dynamic framework that continually learns, and updates parameters based on new feedback, and (ii) comprehensive consideration of the risk of leaks and its escalated accidents are effective in developing safety measures, reducing response time, and minimizing potential damage. Future work should focus on establishing a comprehensive physical leakage model by model in terms of hydrogen corrosiveness, limited space, and embrittlement issues and developing model-and-data driven risk analysis approach to enhance reliability and accuracy of the results.

Acknowledgements

This paper is funded by the Horizon Europe Marie Skłodowska-Curie Postdoctoral Fellowship [DROMS-FOWT – 101146961), UKRI (EPSRC EP/Z001501/1), and the National Natural Science Foundation of China (72301299). This work also contributes to the Strategic Research Plan of the Centre for Marine Technology and Ocean Engineering (CENTEC), which is financed by the Portuguese Foundation for Science and Technology (Fundação para a Ciência e Tecnologia - FCT) under contract UIDB/UIDP/00134/2020.

617 Appendix A. 150 credible leakage scenarios.

Code	Wind speed (m/s)	Wind direction (°)	Leak position	Leak rate (kg/s)	Leak direction	Code	Wind speed (m/s)	Wind direction (°)	Leak position	Leak rate (kg/s)	Wind speed (m/s)
1	8.05	113.29	X4Y1	0.71	-Z	76	11.99	314.36	X3Y1	0.29	-Z
2	5.73	342.35	X4Y1	0.89	+Z	77	11.57	162.38	X4Y1	1.39	-Z
3	16.49	177.63	X4Y3	1.84	-Z	78	12.09	248.92	X3Y1	0.14	+Y
4	0.16	165.08	X4Y2	1.46	+Y	79	18.08	275.38	X3Y1	0.27	-X
5	15.84	168.46	X4Y1	0.68	+Z	80	9.73	121.95	X1Y2	0.38	-Y
6	10.44	44.18	X4Y2	0.32	+Z	81	14.26	287.72	X3Y1	0.98	+X
7	8.92	267.86	X4Y1	0.54	-Z	82	0.98	61.17	X4Y1	1.99	+Z
8	6.92	195.36	X4Y2	0.37	+Y	83	19.19	117.17	X1Y2	1.18	+Z
9	7.25	151.35	X3Y1	0.03	+Z	84	4.24	376.41	X4Y2	0.92	-Z
10	5.02	93.00	X4Y2	1.10	+Y	85	10.02	148.84	X4Y1	14.80	+Y
11	9.41	34.50	X4Y2	0.96	-X	86	9.00	357.04	X4Y3	0.77	+Y
12	2.48	91.99	X1Y2	0.33	+X	87	12.61	142.84	X4Y1	0.76	-X
13	1.89	31.29	X4Y1	0.81	-X	88	4.87	258.88	X1Y2	0.18	-X
14	8.49	254.49	X4Y3	1.95	-Y	89	7.15	250.62	X4Y1	0.65	-Z
15	15.51	331.78	X3Y1	1.49	-Y	90	8.26	53.96	X4Y3	1.67	+Z
16	9.14	3.28	X4Y3	0.21	+Z	91	10.85	190.39	X4Y1	0.47	+Z
17	12.46	185.79	X4Y3	1.61	-X	92	3.13	26.96	X1Y2	0.48	-Y
18	9.54	225.00	X4Y3	0.84	-Y	93	10.08	362.04	X4Y1	1.05	-X
19	17.11	200.16	X4Y1	1.70	-Z	94	16.27	156.56	X4Y2	0.69	+Z
20	7.35	203.02	X4Y3	1.87	-Y	95	8.20	174.88	X4Y1	1.14	+X
21	8.63	52.07	X4Y2	0.74	-Y	96	2.36	126.19	X4Y1	1.53	-X
22	10.39	124.49	X4Y1	0.40	+Y	97	8.02	127.61	X1Y2	0.87	+Y
23	6.39	85.26	X4Y2	0.20	-X	98	12.80	232.44	X1Y2	0.00	+X
24	13.93	40.09	X4Y3	0.55	+Y	99	7.68	280.36	X4Y1	1.28	+X
25	14.71	172.49	X4Y1	0.57	-Z	100	6.66	330.54	X4Y3	0.36	-Z
26	9.30	308.50	X3Y1	0.56	+Z	101	14.05	281.96	X3Y1	1.92	+Y
27	7.21	152.79	X3Y1	0.52	+Y	102	6.10	45.17	X4Y3	1.82	+X
28	7.93	89.64	X3Y1	0.34	-Y	103	9.96	83.26	X4Y1	1.74	+Z
29	4.46	214.00	X1Y2	1.30	-Y	104	17.85	100.32	X4Y2	0.73	+Y
30	9.44	163.88	X4Y1	0.79	+X	105	9.15	178.70	X1Y2	0.60	+Y
31	1.66	254.80	X4Y2	0.88	+X	106	11.54	243.47	X4Y2	0.26	-Z
32	4.19	160.05	X4Y2	0.36	-X	107	13.40	139.78	X4Y2	0.22	+Y
33	12.96	133.84	X4Y1	0.42	+Y	108	1.24	309.06	X4Y1	0.85	+Z
34	3.62	171.87	X1Y2	0.03	-X	109	8.57	103.07	X4Y3	0.08	+X
35	9.84	222.93	X3Y1	0.65	-X	110	6.50	145.40	X4Y3	1.96	-X
36	2.79	78.97	X3Y1	0.54	+Z	111	4.57	165.85	X3Y1	0.39	-Z
37	11.24	217.87	X4Y3	0.31	+Y	112	10.35	263.51	X4Y1	0.13	+X

38	4.98	265.28	X4Y2	1.21	-X	113	12.57	96.18	X4Y1	0.26	+Y
39	14.58	10.61	X4Y1	0.93	-X	114	3.73	158.71	X1Y2	0.24	-X
40	5.48	141.66	X4Y2	0.91	+Z	115	5.60	74.09	X4Y1	17.88	+X
41	13.67	270.76	X4Y1	0.41	-Y	116	7.82	107.40	X4Y1	1.42	+X
42	9.03	123.59	X4Y1	0.64	+Y	117	12.10	245.18	X4Y3	1.35	-X
43	6.33	68.17	X1Y2	1.22	-Y	118	5.62	55.89	X3Y1	0.83	-Y
44	8.16	259.82	X4Y1	0.67	-Z	119	11.44	130.04	X3Y1	0.49	-Z
45	11.36	71.84	X4Y2	1.12	-Y	120	4.38	237.79	X4Y3	0.95	+Z
46	13.34	199.93	X4Y2	0.91	+X	121	15.33	49.65	X1Y2	0.18	-Z
47	6.18	230.03	X4Y2	0.59	+Z	122	6.98	180.55	X4Y1	0.50	-Z
48	5.22	136.14	X4Y1	0.41	+X	123	12.89	204.11	X4Y1	0.46	-Y
49	7.48	134.67	X1Y2	0.85	-Y	124	5.90	62.34	X4Y2	1.26	-Z
50	6.84	118.77	X4Y3	0.45	+X	125	3.31	241.41	X1Y2	0.53	+X
51	9.61	132.22	X4Y2	1.02	-Y	126	10.66	98.53	X1Y2	0.45	+Y
52	5.98	322.68	X4Y1	12.83	-X	127	7.74	67.51	X4Y2	0.29	+Y
53	8.32	211.77	X4Y3	0.68	+Z	128	7.40	188.09	X1Y2	0.07	+X
54	10.90	64.96	X4Y2	1.87	+X	129	14.30	146.31	X4Y2	19.52	+Z
55	13.55	297.93	X4Y2	0.44	-Z	130	3.41	154.56	X4Y2	1.04	-X
56	10.58	169.00	X4Y2	0.16	+Z	131	8.80	293.72	X3Y1	0.30	+X
57	8.81	210.74	X4Y2	0.94	-X	132	11.17	4.28	X3Y1	1.00	+X
58	7.07	155.05	X4Y1	0.15	+X	133	13.12	147.45	X4Y2	0.01	+X
59	7.85	226.16	X4Y3	0.74	+Y	134	10.21	182.46	X3Y1	0.71	+X
60	10.68	109.75	X4Y2	0.63	-Y	135	5.80	438.84	X1Y2	0.27	-Z
61	10.26	221.00	X4Y3	0.10	-Z	136	11.10	176.29	X4Y1	0.62	+Z
62	7.59	237.08	X4Y2	1.63	+X	137	3.96	87.16	X3Y1	0.79	+Y
63	12.24	198.18	X4Y1	0.82	-X	138	13.21	138.86	X3Y1	0.17	-X
64	0.63	235.32	X4Y2	0.98	+Z	139	3.91	21.01	X4Y1	0.51	+Z
65	14.83	216.60	X4Y2	1.45	-Y	140	5.24	111.91	X4Y2	1.72	-Z
66	8.72	302.57	X1Y2	1.35	-X	141	11.04	207.43	X3Y1	1.76	-Y
67	9.86	219.58	X4Y2	0.10	-X	142	6.28	193.30	X4Y1	0.24	-X
68	12.30	105.29	X3Y3	0.95	+Z	143	9.65	191.26	X4Y1	1.58	-Y
69	5.40	247.14	X1Y2	0.76	+Z	144	1.40	105.17	X4Y2	0.08	-Z
70	4.72	26.75	X4Y2	0.80	-Z	145	6.78	194.51	X4Y2	0.59	-Z
71	15.07	77.72	X3Y3	0.89	-Z	146	11.69	278.66	X1Y2	0.60	+X
72	11.73	229.62	X4Y1	0.11	+Y	147	10.79	11.35	X4Y1	0.04	-Y
73	6.59	186.35	X4Y2	1.57	-Y	148	2.62	183.50	X4Y3	0.05	+Y
74	9.24	205.97	X4Y2	0.06	+Y	149	8.42	115.82	X4Y1	0.14	+Z
75	3.64	290.39	X4Y3	0.20	-Y	150	11.85	209.03	X4Y3	0.70	-Y

618

Appendix B. Leakage probability of components under different leak sizes [16].

Storage tank		Heat exchanger		Pump		Valves		Filter		Pipe	
Leak size	Leak probability	Leak size	Leak probability	Leak size	Leak probability	Leak size	Leak probability	Leak size	Leak probability	Leak size	Leak probability
1.00	1.00	1.00	1.00	1.00	1.00	1.00	1.00	1.00	1.00	1.00	1.00
2.04	0.76	2.03	0.60	2.02	0.47	2.00	0.45	2.01	0.37	2.01	0.42
3.03	0.65	3.02	0.45	3.00	0.30	2.98	0.28	2.97	0.21	3.00	0.25
4.00	0.58	3.99	0.36	4.05	0.22	3.96	0.20	4.02	0.13	3.91	0.17
5.09	0.53	4.98	0.31	5.07	0.17	4.98	0.16	4.97	0.10	4.97	0.13
6.15	0.50	6.06	0.27	6.13	0.14	5.92	0.13	6.04	0.08	6.05	0.10
7.11	0.47	7.17	0.24	6.89	0.12	7.05	0.11	6.95	0.06	6.92	0.08
7.95	0.45	8.01	0.22	7.97	0.10	8.01	0.09	7.96	0.05	7.79	0.07
9.15	0.43	9.06	0.20	8.97	0.09	9.17	0.08	9.16	0.05	8.96	0.06
10.17	0.41	10.13	0.18	10.04	0.08	9.81	0.07	9.85	0.04	9.97	0.06
19.91	0.31	20.42	0.11	20.25	0.04	20.13	0.03	19.77	0.01	19.90	0.03
30.15	0.27	30.42	0.08	29.84	0.03	29.67	0.02	30.16	0.01	29.83	0.02
40.80	0.24	40.74	0.07	39.98	0.02	40.20	0.01	40.41	0.01	39.74	0.01
50.78	0.22	50.72	0.05	50.06	0.01	50.32	0.00	50.33	0.01	50.04	0.00
60.77	0.20	61.41	0.05	59.95	0.02	58.25	0.00	59.91	0.00	—	—
70.32	0.19	70.66	0.04	70.56	0.01	69.77	0.01	71.75	0.01	—	—
80.01	0.18	79.51	0.04	80.33	0.01	80.30	0.00	80.29	0.00	—	—
92.07	0.18	90.49	0.03	88.87	0.01	—	—	89.87	0.00	—	—
100.72	0.17	102.99	0.03	99.46	0.01	—	—	98.89	0.00	—	—

References

[1] Jo W, Bae J, Kim D-S, Lee SJ. Automatic accident sequence generation using optimized simulations for dynamic probabilistic safety assessment. Reliability Engineering & System Safety. 2026;266:111643.

[2] Kang Y, Wu W, Xu Y, Liu N. Exploring the perspective of time: A framework for dynamic assessment of leakage risk in WDNs based on a joint model of survival analysis and machine learning. Reliability Engineering & System Safety. 2025;264:111294.

[3] Liu J, Tan L, Ma Y. An integrated risk assessment method for urban areas due to chemical leakage accidents. Reliability Engineering & System Safety. 2024;247:110091.

[4] Ma X, Tsai Y-T, Shu C-M, Yang Y. Risk evolution analysis of gas leakage accidents based on complex network. Safety Science. 2025;182:106692.

[5] Qian C, Li Y, Zhu Y, Yang D, Ren Y, Xia Q, et al. Remaining useful life prediction considering correlated multi-parameter nonlinear degradation and small sample conditions. Computers & Industrial Engineering. 2025;210:111567.

[6] Li M-W, Xu R-Z, Yang Z-Y, Yeh Y-H, Hong W-C. Optimizing berth-crane allocation considering tidal effects using chaotic quantum whale optimization algorithm. Applied Soft Computing. 2024;162:111811.

[7] Xie Q, Zhou T, Wang C, Zhu X, Ma C, Zhang A. An integrated uncertainty analysis method for the risk assessment of hydrogen refueling stations. Reliability Engineering & System Safety. 2024;248:110139.

[8] Yang Z-Y, Cao X, Xu R-Z, Hong W-C, Sun S-L. Applications of chaotic quantum adaptive satin bower bird optimizer algorithm in berth-tugboat-quay crane allocation optimization. Expert Systems with Applications. 2024;237:121471.

[9] B B, George P, Renjith VR, Kurian AJ. Application of dynamic risk analysis in offshore drilling processes. Journal of Loss Prevention in the Process Industries. 2020;68:104326.

[10] Abohamzeh E, Salehi F, Sheikholeslami M, Abbassi R, Khan F. Review of hydrogen safety during storage, transmission, and applications processes. Journal of Loss Prevention in the Process Industries. 2021;72:104569.

[11] Casamirra M, Castiglia F, Giardina M, Lombardo C. Safety studies of a hydrogen refuelling station: Determination of the occurrence frequency of the accidental scenarios. International Journal of Hydrogen Energy. 2009;34:5846-54.

[12] Feng K, Xiao H, Zhang J, Ni Q. A digital twin methodology for vibration-based monitoring and prediction of gear wear. Wear. 2025;571:205806.

[13] Wei F, Tan L, Ma X, Xiao H, Patel D, Lee C-G, et al. A hybrid prognostic framework: Stochastic degradation process with adaptive trajectory learning to transfer historical health knowledge. Mechanical Systems and Signal Processing. 2025;224:112171.

[14] Durga Rao K, Gopika V, Sanyasi Rao VVS, Kushwaha HS, Verma AK, Srividya A. Dynamic fault tree analysis using Monte Carlo simulation in probabilistic safety assessment. Reliability Engineering & System Safety. 2009;94:872-83.

[15] Meng, H., Hu, M., Kong, Z., Niu, Y., Liang, J., Nie, Z., & Xing, J. (2024). Risk analysis of lithium-ion battery accidents based on physics-informed data-driven Bayesian networks. Reliability Engineering & System Safety, 251, 110294.

[16] Kong X, Li H, Guedes Soares C. Grey-based failure mode and effect analysis of floating offshore wind turbines. Ocean Engineering. 2026;343:123353.

[17] Xie C, Huang L, Wang R, Deng J, Shu Y, Jiang D. Research on quantitative risk assessment of fuel leak of LNG-fuelled ship during lock transition process. Reliability Engineering & System Safety. 2022;221:108368.

[18] Meng H, An X, Xing J. A data-driven Bayesian network model integrating physical knowledge for prioritization of risk influencing factors. Process Safety and Environmental Protection. 2022;160:434-49.

[19] Spouge J. New generic leak frequencies for process equipment. Process Safety Progress. 2005;24:249-57.

673 [20] LaChance J, Houf W, Middleton B, Fluer L. Analyses to support development of risk-informed
674 separation distances for hydrogen codes and standards. No. SAND2009-0874. Sandia National
675 Laboratories (SNL), CA (United States), 2009.
676 [21] Zhang B, Liu Y, Wu S. Inspection policy optimization for hierarchical multistate systems under
677 uncertain mission scenarios: A risk-averse perspective. IISE Transactions. 2025;57:213-29.
678 [22] Zheng YX, Zhang B, Liu Y. Reliability Assessment of Reconfigurable k-out-of-n Systems With
679 Functional Dependency. IEEE Transactions on Reliability. 2025;74:3745-59.
680 [23] Bi S, Yun Q, Zhao Y, Wang H. Stochastic model calibration with image encoding: Converting
681 high-dimensional sequential responses into RGB images for neural network inversion.
682 Mechanical Systems and Signal Processing. 2025;230:112606.
683 [24] Ji G, Cai B, Liu X, Jiang Y, Zhao Y, Li Q, et al. Leakage localization methodology based on
684 dynamic pressure signal for subsea pipeline. Engineering Applications of Artificial Intelligence.
685 2025;161:112212.
686 [25] Hecht E, Ehrhart B, Groth KM. Hydrogen Plus Other Alternative Fuels Risk Assessment Models
687 (HyRAM+) (Technical Reference Manual V.4). United States, 2021.
688 [26] Villa V, Paltrinieri N, Khan F, Cozzani V. Towards dynamic risk analysis: A review of the risk
689 assessment approach and its limitations in the chemical process industry. Safety Science.
690 2016;89:77-93.
691 [27] Huang H-Z, Li H, Shi Y, Huang T, Yang Z, He L, et al. Theory and application of possibility and
692 evidence in reliability analysis and design optimization. Journal of Reliability Science and
693 Engineering. 2025;1:015007.
694 [28] Huang T, Zhang Q, Beer M, Liu Y, Huang H-Z. A dynamic reliability assessment method for
695 multi-state manufacturing system by merging imprecise observational information. Reliability
696 Engineering & System Safety. 2026;266:111722.
697 [29] Kong X, Dong Y, Kang J, Paik JK. Quantitative Risk Assessment and Management of Hydrogen
698 Leaks from Offshore Rocket Launching Platforms. In: 2023 9th International Symposium on
699 System Security, Safety, and Reliability (ISSSR); 2023:149-55.

[30] Jin T, Wu M, Liu Y, Lei G, Chen H, Lan Y. CFD modeling and analysis of the influence factors of liquid hydrogen spills in open environment. International Journal of Hydrogen Energy. 2017;42:732-9.

[31] Meng X, Chen G, Zhu G, Zhu Y. Dynamic quantitative risk assessment of accidents induced by leakage on offshore platforms using DEMATEL-BN. International Journal of Naval Architecture and Ocean Engineering. 2019;11:22-32.

[32] Wang W, Zhang Y, Li Y, Hu Q, Liu C, Liu C. Vulnerability analysis method based on risk assessment for gas transmission capabilities of natural gas pipeline networks. Reliability Engineering & System Safety. 2022;218:108150.

[33] Ning F, Cheng Z, Meng D, Duan S, Wei J. Enhanced spectrum convolutional neural architecture: An intelligent leak detection method for gas pipeline. Process Safety and Environmental Protection. 2021;146:726-35.

[34] Kopbayev A, Khan F, Yang M, Halim SZ. Gas leakage detection using spatial and temporal neural network model. Process Safety and Environmental Protection. 2022;160:968-75.

[35] Zhang H, Wen B, Tian X, Li X, Dong Y, Wang M, et al. Experimental study on mitigating vibration of floating offshore wind turbine using tuned mass damper. Ocean Engineering. 2023;288:115974.

[36] Qiu S, Chen B, Wang R, Zhu Z, Wang Y, Qiu X. Atmospheric dispersion prediction and source estimation of hazardous gas using artificial neural network, particle swarm optimization and expectation maximization. Atmospheric Environment. 2018;178:158-63.

[37] Pérez-Pérez EJ, López-Estrada FR, Valencia-Palomo G, Torres L, Puig V, Mina-Antonio JD. Leak diagnosis in pipelines using a combined artificial neural network approach. Control Engineering Practice. 2021;107:104677.

[38] George PG, Renjith VR. Evolution of Safety and Security Risk Assessment methodologies towards the use of Bayesian Networks in Process Industries. Process Safety and Environmental Protection. 2021;149:758-75.

[39] Li H, Díaz H, Soares CG. A failure analysis of floating offshore wind turbines using AHP-FMEA methodology. Ocean Engineering. 2021;234:109261.

[40] Li H, Diaz H, Soares CG. A developed failure mode and effect analysis for floating offshore wind turbine support structures. Renewable Energy. 2021;164:133-45.
[41] Li H, Soares CG. Assessment of failure rates and reliability of floating offshore wind turbines. Reliability Engineering & System Safety. 2022;228:108777.
[42] Kong X, Kang J, Li H, Dong Y, Kang HS. Risk analysis of offshore rocket launch propellant filling system under data and knowledge scarcities. Ocean Engineering. 2024;300:117435.
[43] Tchouvelev AV. Knowledge gaps in hydrogen energy. A white paper. Revision 1. 2008.
[44] Cao XH, Stojkovic I, Obradovic Z. A robust data scaling algorithm to improve classification accuracies in biomedical data. BMC Bioinformatics. 2016;17:359.
[45] Zhang X, Shi J, Li J, Huang X, Xiao F, Wang Q, et al. Hydrogen jet and diffusion modeling by physics-informed graph neural network. Renewable and Sustainable Energy Reviews. 2025;207:114898.
[46] Xu Z, Saleh JH. Machine learning for reliability engineering and safety applications: Review of current status and future opportunities. Reliability Engineering & System Safety. 2021;211:107530.
[47] He X, Kong D, Yang G, Yu X, Wang G, Peng R, et al. Hybrid neural network-based surrogate model for fast prediction of hydrogen leak consequences in hydrogen refueling station. International Journal of Hydrogen Energy. 2024;59:187-98.
[48] Niaz S, Manzoor T, Pandith AH. Hydrogen storage: Materials, methods and perspectives. Renewable and Sustainable Energy Reviews. 2015;50:457-69.
[49] Fang H, Xue H, Tang W. A new approach for quantitative risk assessment of gas explosions on FPSO. Ocean Engineering. 2022;260:112006.
[50] Selvaggio AZ, Sousa FMM, Silva FVd, Vianna SSV. Application of long short-term memory recurrent neural networks for localisation of leak source using 3D computational fluid dynamics. Process Safety and Environmental Protection. 2022;159:757-67.
[51] Tian W, Jin M, de Wilde P, Fu X, Li G. Uncertainty analysis of building energy analysis based on replicated Latin Hypercube sampling. Building Simulation 2021: IBPSA; 2021:1303-10.
[52] Lee W. A pressure iteration scheme for two-phase flow modeling. 1980;1:407-31.

[53] Houf W, Schefer R. Analytical and experimental investigation of small-scale unintended releases of hydrogen. International Journal of Hydrogen Energy. 2008;33:1435-44.

[54] Stamatelatos M, Dezfuli H, Apostolakis G, Everline C, Guarro S, Mathias D, et al. Probabilistic risk assessment procedures guide for NASA managers and practitioners. 2011.

[55] Mulcahy GW, Brooks DM, Ehrhart BD. Using Bayesian Methodology to Estimate Liquefied Natural Gas Leak Frequencies. Sandia National Lab. (SNL-NM), Albuquerque, NM (United States); 2021

[56] ISO 19880-1:2020. Gaseous-fuelling stations-Part 1: general requirements. Geneva, Switzerland: International Organization for Standardization.

[57] Wang M, Han F, Li H, Zhou J, Wang Z. Reliability and Risk Assessment of Hydrogen-Powered Marine Propulsion Systems Based on the Integrated FAHP-FMECA Framework. 2025;13:2115.

[58] Hoang AT, Pandey A, Martinez De Osés FJ, Chen W-H, Said Z, Ng KH, et al. Technological solutions for boosting hydrogen role in decarbonization strategies and net-zero goals of world shipping: Challenges and perspectives. Renewable and Sustainable Energy Reviews. 2023;188:113790.

[59] Rodríguez Castillo CA, Collu M, Brennan F. Design considerations and preliminary hydrodynamic analysis of an offshore decentralised floating wind-hydrogen system. International Journal of Hydrogen Energy. 2024;89:496-506.

[60] He X, Kong D, Yu X, Ping P, Wang G, Peng R, et al. Prediction model for the evolution of hydrogen concentration under leakage in hydrogen refueling station using deep neural networks. International Journal of Hydrogen Energy. 2024;51:702-12.

[61] Zhang X, Shi J, Li J, Huang X, Xiao F, Wang Q, et al. Hydrogen jet and diffusion modeling by physics-informed graph neural network. Renewable and Sustainable Energy Reviews. 2025;207:114898.